AD-A268 402

A Mechanical System Damping Measurement Technique Using a One-Degree-of-Freedom (1DOF) Cylindrical Gas Bearing

C. L. Ratliff and E. J. Marquart
Calspan Corporation/AEDC Operations

DTIC
ELECTE
AUG 2 4 1993
B

August 1993

Final Report for Period February 13 through September 30, 1992

93-19540

93 8 23 033

ARNOLD ENGINEERING DEVELOPMENT CENTER
ARNOLD AIR FORCE BASE, TENNESSEE
AIR FORCE MATERIEL COMMAND
UNITED STATES AIR FORCE

APPROVAL STATEMENT

This report has been reviewed and approved.

J. W. CAMPBELL, Capt, USAF
Aerophysics Systems Flight
Aerospace Flight Dynamics Test Division
Test Operations Directorate

Approved for publication:

FOR THE COMMANDER

DENNIS N. HUPRICH, Maj, USAF
Chief, Aerospace Systems Flight
Aerospace Flight Dynamics Test Division
Test Operations Directorate

REPORT DOCUMENTATION PAGE

1. AGENCY USE ONLY (Leave blank)	2. REPORT DATE August 1993	3. REPORT TYPE AND DATES COVERED Final Report for Feb. 13 - Sept. 30, 1992

4. TITLE AND SUBTITLE A Mechanical System Damping Measurement Technique Using a One-Degree-of-Freedom (1DOF) Cylindrical Gas Bearing	5. FUNDING NUMBERS PN - 0328
6. AUTHOR(S) Ratliff, C. L. and Marquart, E. J. Calspan Corporation/AEDC Operations	

7. PERFORMING ORGANIZATION NAME(S) AND ADDRESS(ES) Arnold Engineering Development Center/DOF Air Force Materiel Command Arnold Air Force Base, TN 37389-4000	8. PERFORMING ORGANIZATION REPORT NUMBER AEDC-TR-93-10

9. SPONSORING/MONITORING AGENCY NAMES(S) AND ADDRESS(ES) Arnold Engineering Development Center/DOFR Air Force Materiel Command Arnold Air Force Base, TN 37389-4405	10. SPONSORING/MONITORING AGENCY REPORT NUMBER
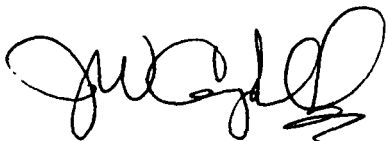
11. SUPPLEMENTARY NOTES   Available in Defense Technical Information Center (DTIC).

12a. DISTRIBUTION/AVAILABILITY STATEMENT Approved for public release; distribution is unlimited.	12b. DISTRIBUTION CODE

13. ABSTRACT (Maximum 200 words)

An experimental investigation was conducted in the Airflow Calibration Laboratory (ACL) to separate the total rolling moment of rigid and nonrigid mechanical systems into viscous damping and coulomb rolling-moment components. The test technique consisted of measuring roll rate decay of these rigid and nonrigid mechanical systems on a one-degree-of-freedom (1DOF) cylindrical gas bearing. To better understand the 1DOF bearing tare damping, a significant amount of information was collected about the operational characteristics of the 1DOF cylindrical gas bearing at certain test conditions. The 1DOF bearing characteristics and test technique are described in this report. The application of the test technique developed for this investigation could be beneficial for determining damping properties of other mechanical systems such as turbomachinery, space structures, gas/ball bearings, and high-damping-capacity materials. The primary measurement uncertainties for the present investigation were determined as follows: ± 0.01 deg/sec for roll rate obtained with a one-spot tachometer ring, ± 0.001 in.-lbf for viscous damping moment, or, in terms of energy dissipation, ± 1 mW. The coulomb rolling-moment uncertainty could not be established because of its variable nature.

14. SUBJECT TERMS mechanical damping, viscous damping moment, coulomb rolling moment, roll, gas bearing, structural damping, film gap, tare, moment of inertia, energy dissipation, rigid and nonrigid	15. NUMBER OF PAGES 51
	16. PRICE CODE

17. SECURITY CLASSIFICATION OF REPORT UNCLASSIFIED	18. SECURITY CLASSIFICATION OF THIS PAGE UNCLASSIFIED	19. SECURITY CLASSIFICATION OF ABSTRACT UNCLASSIFIED	20. LIMITATION OF ABSTRACT SAME AS REPORT

PREFACE

DTIC QUALITY INSPECTED 3

Accession For

NTIS GRA&I ☑
DTIC TAB ☐
Unannounced ☐
Justification

By

Distribution/

Availability Codes

Dist | Avail and/or
     | Special

A-1

CONTENTS

ILLUSTRATIONS

TABLES

1.0 INTRODUCTION

An experimental investigation was conducted in the Airflow Calibration Laboratory (ACL) to separate the total rolling moment of rigid and nonrigid mechanical systems into viscous damping and coulomb rolling-moment components. The test technique consisted of measuring roll rate decay of a rigid and nonrigid engineering unit dissipator (EUD) on a one-degree-of-freedom (1DOF) cylindrical gas bearing. A 1DOF gas bearing is a gas film-lubricated pivot which provides excellent high load carrying capacity, low frictional torque or damping moment, and unlimited rotation. Gas bearings have been used at AEDC for obtaining pitch and yaw dynamic stability measurements since 1962 (Ref. 1) and three-degree-of-freedom (spherical bearing) measurements since 1967 (Ref. 2).

Applications of gas bearings are almost unlimited, and the designs are continually being changed for maximum operating performance. The current investigation utilized a 1969 AEDC-designed 1DOF gas bearing (Ref. 3) enhanced with up-to-date instrumentation. A rigid EUD was used to establish a tare with deviations produced by various levels of internal damping of the nonrigid EUD. The term *tare* refers to the moment to be deducted from all other data. For some classes of aerodynamic configurations at hypersonic speeds, the tare damping moment can approach or even exceed the aerodynamic damping moments (Ref. 4). Mechanical systems can also have similar degrees of damping. Therefore, the degree of accuracy in obtaining viscous damping and coulomb rolling-moment measurements depends upon the accuracy of the 1DOF bearing tare damping. To better understand the 1DOF bearing tare damping, a significant amount of information was collected about the operational characteristics of the 1DOF cylindrical gas bearing at certain test conditions. The 1DOF bearing characteristics and test technique are described in this report. The application of the test technique developed for this investigation could be beneficial for determining damping properties of other mechanical systems such as turbomachinery, space structures, gas/ball bearings, and high damping capacity materials.

Unconventional methods were required to evaluate mechanical system damping with a 1DOF gas bearing that is typically used for wind tunnel testing. These methods affected the operation, instrumentation, data acquisition, and data reduction for the 1DOF bearing. The particular bearing selected for the investigation was found to be sensitive to environmental disturbances, including but not limited to bearing temperature, bearing pressure, ambient chamber pressure, external vibration, and applied loads. These disturbances were discernable in the present data measurements because of the improved instrumentation accuracy. Previous wind tunnel tests that used the 1DOF bearing did not discern the subtle characteristics because the damping measurements and data uncertainties were relatively large. The primary measurement uncertainties for the present investigation were determined as follows: ±0.01 deg/sec for roll rate obtained with a one-spot tachometer ring, ± 0.001 in.-lbf for viscous

damping moment or, in terms of energy dissipation, ± 1 milliwatt (mW); the coulomb rolling-moment uncertainty could not be established because of its variable nature.

2.0 APPARATUS

2.1 FACILITY

2.1.1 Airflow Calibration Laboratory (ACL)

The Airflow Calibration Laboratory (ACL) is a circular chamber approximately 7.4 ft in diameter by 12 ft long (Fig. 1). Originally designed as a low-density hypersonic tunnel, the ACL chamber has been modified to serve as a calibration and mechanics laboratory. With minor modifications, the ACL can provide calibrations for hardware such as inlet/nozzle models, air-powered turbine engine simulators, flow-field pressure probes, and hot-wire (or hot-film) anemometer probes. The chamber shell is hydraulically driven on a set of rails to allow for easy access during model installation, changes, and removal. The chamber is securely locked in place with handclamps against a rigid bulkhead. O-rings at the bulkhead and at the exhaust duct are used to minimize air in-leakage during vacuum operations. Viewing ports in the chamber are available for visual and/or photographic coverage. A pneumatically operated valve is used to open and close a 35-in.-diam exhaust duct approximately 60 ft downstream of the chamber. A separate valve is used to exhaust or vent the chamber to atmosphere.

2.1.2 Vacuum Pump

Subatmospheric chamber pressures of approximately 0.02 psia can be obtained if no mass flow addition is required and 0.5 psia with the maximum allowable flow rate addition of 0.05 lbm/sec with both the mechanical and booster pump operating. The Stokes® vacuum pump (model 1711) provides a maximum pumping speed of 1,100 cfm to obtain these lower chamber vacuum pressures. At the maximum mass flow rate addition, the chamber can be pumped down in approximately 30 min. Evacuation of ACL with the AEDC Main Compressor Plant is an available option, but depending on test requirements, objectives, and cost, the Stokes vacuum pump may be preferred.

2.2 HARDWARE

2.2.1 1DOF Gas Bearing

The AEDC 1DOF gas bearing fabricated in 1969 is approximately 8 in. long by 2.5 in. in. in diameter; it is ideal for obtaining roll damping measurements because of its near-frictionless rolling resistance (Fig. 2). The 1DOF bearing is composed of a journal and thrust

bearing. High-pressure air is supplied to the plenum chamber of the bearings. This high-pressure air is forced through the orifices that are drilled into the bearing surfaces. Normal loads are supported by the journal bearing. Orifices are located on both sides of the thrust bearing to support positive and negative axial loads. An outer cylindrical race houses the inner bearings with less than 0.001-in. clearance. The outer cylinder contains the high-pressure air, with the exception of several vent holes. The rotating parts were made from 440B stainless, the thrust bearing core was made from Armco® PH 13-8 Mo. stainless steel, and the journal inner core was Kennertium-W2® . A sleeve (not shown in Fig. 2) slides over the outer race and is pinned to serve as a model adaptor. The average designed film gaps for the journal and thrust bearing are 0.00076 and 0.00072 in., respectively. The orifices are machined without a recess to avoid pneumatic hammer instabilities (Ref. 3) resulting from turbulent gas film flow. The combination of small orifices and minimum film gap provides increased gas flow resistance or "film stiffness" and maintains laminar flow.

2.2.2 Tare Model

The tare model was a rigid hollow-cylindrical body with two internal bulkheads located forward and aft of the 1DOF bearing sleeve. A typical model configuration (Fig. 3) included a turbine ring fixed to the rear of the tare cylinder, a spool, an EUD (rigid or nonrigid), and counterweight balance rings. The symmetric turbine vanes were designed to avoid bias damping moments independent of spin direction. A miniature converging-diverging contoured nozzle provided supersonic flow to the turbine vanes for various model spin rates. The spool was mounted adjacent to the turbine vanes as a reference for obtaining roll moment of inertia measurements (Section 4.4). The model was designed to be balanced at the center of the journal bearing. To compensate for the weight addition of an EUD installed in the front cavity of the cylinder, brass counterweight rings were added to the rear of the model to properly balance the total weight over the center of the journal bearing (Fig. 2). Total weight for configurations including an EUD, counterweight(s), and tare model was either 183 or 300 lbf.

2.2.3 Engineering Unit Dissipator (EUD)

Two rigid engineering unit dissipator (EUD) models were fabricated with different weights for establishing 1DOF bearing tares at the same weight as the nonrigid EUD models. The nonrigid EUD models were fabricated with features to produce various internal viscous damping moments within the EUD shell (Fig. 3).

7

2.3 INSTRUMENTATION

2.3.1 Data Acquisition

The data consisted of roll rate, time, bearing supply pressure and temperature, chamber pressure, dewpoint temperature of the bearing air supply, mass flow rate, and bearing wall temperature which were recorded with a Gateway® 2000 486DX/33E PC-based unit located in the ACL control room. All PC support software was National Instruments® LabWindows®. The PC was programmed to continuously update the measured bearing and test chamber conditions and display these updates on the video monitor. The most important real-time display was the roll rate decay of the test article via a strip chart. The PC-based data system was capable of collecting data on 16 channels at a rate of 100K samples/sec using a 12-bit resolution A/D board with simultaneous sample-and-hold capability and digital I/O format. To acquire accurate roll rate, the time was counted with very precise Hewlett Packard® (HP) timers once every other revolution. The photodiode sensor was interrupted every revolution from a one-spot tachometer ring that activated corresponding HP timers.

In previous tests, the analog pulse train signal was transmitted from the photodiode sensor to a frequency-to-voltage (F/V) converter that produced an analog voltage proportional to roll rate. The voltage was then digitized and recorded. Typical roll rate uncertainties of $\pm$ 1 deg/sec were not uncommon. This scheme was not acceptable for mechanical system damping measurements which required a energy dissipation resolution of $\pm$ 1 mW. By circumventing the F/V converter instrumentation, the one spot/revolution signal was sent to the accurate HP timers where the pulses open and close timer gates. Every other revolution was recorded by a timer and the data acquisition computer in digital format. Roll rate uncertainties of $\pm$ 0.01 deg/sec were obtained for the investigation. Further data reduction was handled by transmitting the acquired data from the PC to a Sun® workstation via Network Facility Server (NFS) software. Additional engineering data analysis was performed on other office 486 PC's by accessing the Sun workstation hard disk drive by NFS. Estimated uncertainties for the majority of instrumentation are presented in Table 1. The listed instrumentation uncertainties were estimated by using either manufacturers' specifications, calibration against instruments traceable to the National Institute of Standards and Technology, or making the standard deviation calculations from repeat runs.

2.3.2 Journal Bearing Film Gap

Several methods of determining the 1DOF journal bearing film gap were attempted, including the use of dial indicators, height gages wired with a flashlight bulb to indicate surface contact, and a Sony® Magnascan LVDT device. However, the measurement resolution was always greater than the designed film gap. Reference 3 defined the journal bearing film gap

8

to be 0.00076 in. (Ps = 414 psia, Ts = 60°F) and assumed the gap to be constant. The experimental setup in Ref. 3 consisted of a Sheffield® air gage to measure the displacement of the outer race with respect to the journal bearing. In the present investigation, a laser measurement system (HP-5528A) was selected to measure the film gap with an instrument uncertainty of ± 1 ppm of an inch, which was two orders of magnitude better than required. The laser system (Fig. 4) proved to be effective in measuring the gap for both the unloaded and loaded cases.

The 5528A system consists of a display unit (HP-5508A), a laser head (5518A), a linear retroreflector, and an interferometer. The HP-5508A is basically a microprocessor unit and functions as a controller for the pulse counters with an A/D converter and a keyboard/display assembly. The laser head contains an automatically tuned helium-neon laser, circuits to control the laser, and optical receivers. The laser generates a coherent, collimated, two-frequency beam of light. Maximum power output is 1 mW with a wavelength of 632.991 nm. The laser beam is directed through measurement optics and then returned to the receiver. Relative displacement between the measurement optics results in a change of the measurement frequency. The 5508A compares the measurement frequency to the reference frequency and calculates the displacement of the optics. Separate laser/optic configurations were used to measure displacement in the vertical and horizontal plane and were independently confirmed as valid installations. The film gap study revealed some interesting information about the bearing radial spring stiffness (Section 4.3) and provided an acceptable technique for precise gap measurements.

3.0 PROCEDURE

3.1 TEST PREPARATION

The 1DOF bearing and subcomponents were thoroughly cleaned in a sonic bath for several hours. All components were then rinsed, air dried, and assembled with lint-free gloves while maintaining a minimum of 100-psia air supply pressure. The supply pressure air was continuously cleaned using three different size filters in series. The air passed through 10-, 2-, and 0.5-μin. screen filters prior to entering the bearing. This series of filtering reduced the potential for particulate contamination of the film gap which could cause serious damage to the bearing. Next, the tare model was installed on the 1DOF bearing sleeve with several bolts and pin fittings. Minor adjustments were made to true or align the outer surface of the model to within ± 0.002 in. of runout during roll. To adjust for static roll imbalances, combinations of small nuts and bolts were placed at accommodating radial distances to produce countermoments. A brass counterbalance ring(s) was slipped over the front end of the cylindrical model surface and pushed towards the rear (Fig. 3) prior to mounting an EUD. The rings were then secured with Teflon® tip set screws once the total model weight was

9

balanced over the bearing center. The Teflon screws prevented scratches, indentions, and galling of the cylindrical model surface.

3.2 OPERATING CONDITIONS

Nominal operating conditions during data acquisition are presented in Table 2. Roll rate decay data could be obtained by spinning the model clockwise or counterclockwise, as viewed in Fig. 3b, with the model weight balanced at the center of the journal bearing.

3.3 OPERATING PROCUEDURE

Following the initial preparation described in Section 3.1, operating procedures were implemented for a series of test sequences. The downstream valves (Fig. 1) were remotely closed from the ACL control panel. As the 1DOF bearing high-pressure air began to slowly fill the enclosed chamber volume, the Stokes vacuum mechanical pump switch was turned on to start evacuation. Once the chamber ambient pressure reached 1.8 psia the blower pump was activated to augment the mechanical rotary vane pump. The blower pump provided additional pumping speed to achieve a chamber pressure of 0.5 psia. When the minimum chamber pressure was obtained, the jet nozzle was used to initiate the model spin. The additional mass flow from the turbine nozzle was regulated to slowly accelerate the model from rest. When the roll rate reached 720 deg/sec, the jet nozzle was turned off with a remote solenoid valve. The model began to decelerate once the jet nozzle was closed. When the model roll rate decreased to 700 deg/sec, data acquisition was activated by the 486 PC computer program. Data acquisition was terminated when the roll rate reached 180 deg/sec. Typical data acquisition time took about 45 to 60 min from the initial to final roll rate. Upon completion of a data run, all acquired data were transferred to the Sun workstation for final data reduction.

3.4 DATA REDUCTION

This section explains the process of determining the viscous damping and coulomb rolling-moment distribution over the roll rate range of each run. The described technique is used at AEDC (Ref. 5) to determine the damping moments acting on any arbitrary model configuration during spin down. The one-degree-of-freedom roll equation of motion can be written as:

$$\ddot{\phi} I_{xx} = \dot{\phi} \frac{\partial L}{\partial \dot{\phi}} + \phi \frac{\partial L}{\partial \phi} + Lo \qquad (1)$$

By assuming the roll angle dependencies are negligible, Eq. (1) becomes:

$$\ddot{\phi} I_{xx} = \dot{\phi} \frac{\partial L}{\partial \dot{\phi}} + Lo \qquad (2)$$

Equation (2) can be rewritten as a first-order ordinary differential equation (ODE) by substituting $P = \dot{\phi}$ and $\dot{P} = \ddot{\phi}$ into Eq. (2) and rearranging as follows:

$$\dot{P} I_{xx} - P \frac{\partial L}{\partial P} - Lo = 0 \qquad (3)$$

where $\partial L / \partial P = Lp$ is the viscous damping-moment parameter, Lo is the constant coulomb rolling moment, and $\dot{P} I_{xx} = LT$ is the total damping moment. If the total rolling moment is a linear function of P (i.e., $\partial L / \partial P$ and Lo are constant), then Eq. (3) can be solved as a linear ODE with constant coefficients with initial conditions, $\dot{\phi} = P_i$ and $\phi = \phi_i$ at $t = t_i$ with a solution as follows:

$$P(t) = (P_i - P_{ss}) e^{\{(\partial L / \partial P / I_{xx}) t\}} + P_{ss} \qquad (4)$$

where
$$P_{ss} = \frac{-Lo}{\partial L / \partial P}$$

For the case where the coulomb rolling moment is not assumed to be a constant, the differential equation does not have constant coefficients and may not be linear. The approach in determining the coulomb rolling-moment variation with roll rate involves determining the total moment variation and then removing the viscous moment component from the total moment variation.

Equation (3) can be written as Eq. (5) where Lo is replaced with LO as the total nonconstant coulomb rolling moment.

$$LO = \dot{P} I_{xx} - P \frac{\partial L}{\partial P} \qquad (5)$$

The total moment variation with roll rate throughout a run is determined from the model moment of inertia and the roll rate deceleration using Eq. (1) with the right-hand side representing the total moment. The roll rate deceleration at any roll rate is the slope of the roll rate versus time.

Viscous-dominated motion occurs at higher roll rates and coulomb-dominated motion occurs at lower roll rates since viscous moments are, by definition, proportional to roll rate.

The technique used to determine the viscous and coulomb moment distributions involves using only the higher roll rate data to determine the viscous damping-moment parameter. The viscous-dominated roll rate range has an exponential decay, but an engineering judgment is made to determine the roll rate that indicates where viscous-dominated motion transitions to coulomb-dominated motion. The viscous damping-moment parameter $\partial L/\partial P$ is determined by an exponential curve fit to the measured P *versus* t data for all roll rates above the separation roll rate using a differential correction, least-squares technique. An average or constant coulomb rolling moment for the higher roll rate range is also obtained from the curve fit technique.

The coulomb rolling moment in the lower roll rate range can be calculated from Eq. (5). All parameters such as the local roll rate deceleration, roll moment of inertia, and roll rate are known. The relatively small viscous damping moment in the lower roll rate range is estimated by:

$$LP = P\frac{\partial L}{\partial P} \tag{6}$$

A good check on the initial engineering judgment of the separation roll rate is to apply Eq. (5) to the higher roll rate range and determine the range of roll rates where there is agreement of Lo and LO. The present investigation revealed that the roll rate deceleration was exponential (i.e., constant coulomb moment). Therefore, an exponential curve fit was applied to the entire data set of each run. The total viscous damping and coulomb rolling moments calculated using Eqs. (6) and (5), respectively, are composed of contributions from the 1DOF bearing and EUD. To obtain the viscous damping and coulomb rolling moments associated with the nonrigid EUD models, the tare moments of the bearing were subtracted. The viscous and coulomb tare moments were obtained from a rigid body run. Therefore, the total energy dissipation of the EUD is the difference between total damping and the tare model damping.

4.0 RESULTS AND DISCUSSION

4.1 THERMAL EQUILIBRIUM

Initial measurements of the bearing gap with the laser at several values of supply pressure (Ps) indicated nonrepeatable data trends. By increasing supply pressure with constant heat addition, the bearing wall temperature decreased. The expansion of the air through the bearing orifices cooled the bearing as a result of the Joule-Thomson air throttling effect. This Joule-Thomson pressure drop produced a thermal gradient over the bearing which conducted along the sting, resulting in the nonlinear data trends. Therefore, thermal equilibrium was established

prior to exhausting the supply air to atmosphere via a "dump" valve. By dumping the high-pressure air in a few seconds (i.e., collapsing film gap), the risk of bearing temperature changes was minimized. To illustrate the thermal effects on film gap, Fig. 5 is presented with thermal equilibrium requiring at least 30 min while maintaining a constant Ps. When Ps was adjusted to compensate for air supply temperature (Ts) variations for a known gap, the thermal equilibrium process was minimized. The wall temperature was used as a monitoring parameter only, and is not intended to represent the overall bearing temperature distribution.

4.2 UNLOADED FILM GAP PROFILES

The unloaded journal bearing film gap was defined as supporting the weight of the outer race and retroreflector (i.e., 3 lbf). As presented in Fig. 6, at Ps > 100 psia, the film gap reached a maximum clearance where the outer race and journal bearing were concentric for the "no-load" condition. At about 100 psia, there were other gap clearances which depended upon the bearing temperature as discussed in Section 4.1. In Fig. 6, the journal bearing film gap dimension is constant for various supply pressures, but changes for different steady-state wall temperatures. Therefore, maintaining a nearly constant wall temperature was required during a test run to minimize damping perturbations caused from film gap changes. Understanding the characteristics of a bearing prior to testing is important in determining interactions of the bearing with test conditions. Viscous damping moments of air bearings can be reduced by decreasing the supply temperature (Ts). The major effect of reducing Ts for this particular bearing was the reduction in film gap (Fig. 6). As film gap decreases, the viscous damping moment usually increases for constant Ps (Ref. 3). Another interaction factor to consider is that decreasing the film gap will increase radial and angular "stiffness" of the bearing, which increases load capacity (Ref. 1). Therefore, knowing the bearing's interactions can determine what test conditions are important to maintain during testing. The bearing interaction information could also be beneficial in meeting test objectives such as optimizing load capacity rather than reducing viscous damping.

4.3 LOADED FILM GAP PROFILES

The laser measurement technique was found to be beneficial in determining the journal bearing film gap for various applied normal loads. Knowing the film gap for different loads established minimum Ps values for safe operation and possible damping trends. A second bearing was installed during the investigation because it had smaller orifices (i.e., brass inserts) which would reduce the mass flow rate into the ACL chamber and thus allow lower chamber pressures to be obtained. Unfortunately, the second bearing's mass flow rate was not low enough to justify operation, but loaded film gap profiles were obtained to validate the measurement technique. Also, no design or construction details exist for the second 1DOF bearing. Afterwards, the original 1DOF bearing was replaced, and the 1DOF bearing

investigation continued, excluding loaded film gap profiles because of limited time and resources.

An example of several load profiles is presented in Fig. 7 for the second 1DOF bearing. The secondary bearing is insensitive to a large steady-state temperature change ($60 <$ Tw $< 180°$F) as opposed to the trend with the original bearing, which is constructed from common material. The secondary bearing material is 440 B stainless steel. The unloaded gap was measured as 0.00096 in. for $100 <$ Ps < 600 psia. Gap values at approximately 0.00035 in. resulted in signs of grounding on the ohmmeter, thus terminating the profiles at the lower Ps values. Knowing the gap profiles for applied loads, supply pressures, and bearing temperatures can provide additional insight into analyzing data results for any 1DOF gas bearing tests. By using the vertical displacement (Dy) of the journal bearing relative to the unloaded position as a function of supply pressure, the radial spring stiffness characteristics were determined (Fig. 8). As presented in Fig. 8, the journal bearing had a combination of linear and nonlinear attributes depending on Ps. Basically, the radial spring stiffness profiles indicated that increasing supply pressure above 600 psia does not contribute significantly to the gain in normal load capacity, as was the case when Ps was increased from 100 to 200 psia. The radial spring stiffness for the second bearing at Ps = 600 psia was determined to be approximately 8.75×10^5 lbf/in. as indicated in Fig. 8. By experimentally measuring the spring stiffness and moments of inertia, and knowing the model weight, the first natural frequencies can be estimated (Ref. 3). This information can be used to determine whether a bearing can operate at or spin slowly through the natural frequency with a given amount of unbalance (Ref. 3). For the present investigation, the radial and angular frequencies were estimated to be 168 and 20 Hz, respectively. Angular natural frequencies were measured in the range of 10-13 Hz and were not encountered during the investigation, since roll rates were less than 3 Hz.

4.4 ROLL MOMENTS OF INERTIA

The moment of inertia about the roll axes (I_{xx}) was measured experimentally after the tare model was statically balanced in roll. A method commonly used at AEDC for 1DOF systems is the roll acceleration method. As shown in the typical setup presented in Fig. 9, a flexible tungsten 0.012-in.-diam wire was wound tightly and equally spaced per revolution around the spool with the distance from the roll axis to the centerline of the wire accurately measured. One of two different weights was attached to the free end of the wire and released. During the model acceleration the photodiode transmits a signal per each revolution to the HP timer. The time for each of the two revolutions of the model was recorded, and the sequence was repeated.

Equation (7), derived by Smith and Jenke at AEDC in 1975, was used to calculate the model acceleration.

$$a = \frac{4\pi r(P_2 t_1 - P_1 t_2)}{(t_2^2 t_1 - t_1^2 t_2)} \qquad (7)$$

where t_1 is the time through P_1 revolutions, and t_2 is the time through P_2 revolutions. Several drops were made for both weights, and an average acceleration for each weight was determined. Once the average acceleration was known for both weights A and B, Eq. (8) was used to compute I_{xx} as follows:

$$I_{xx} = \frac{r^2}{(a_A - a_B)}\left[(w_A - w_B) - \frac{(w_A a_A - w_B a_B)}{g}\right] \qquad (8)$$

Typical uncertainties for roll moment of inertia measurements in previous tests were between 1 and 1.5 percent. The uncertainty for the present investigation was approximately $\pm$ 0.01 percent, or two orders of magnitude better. Although the roll moment of inertia standard deviation in absolute terms was equivalent to previous test measurements, the improved uncertainty for this investigation can be attributed to the HP timers' accuracy and increased resolution.

4.5 TARE MATH MODEL

As explained in Section 3.4, the energy dissipation of an EUD was determined by subtracting the tare damping from the total system damping. To quantify the tare value at the nominal test conditions (see Table 1), each test condition is individually perturbed about its nominal set point while the other conditions are held constant. The sequence is repeated until all test conditions have been varied. The constants in Eq. (9) are the nominal set points about which test conditions were perturbed. By combining all of the tare study runs into a multiple linear regression code, a total damping equation was defined for the tare model as follows:

$$LT_{Tare} = a_0 + a_1 P + [a_2(P_s - 305) + a_3(P_c - 0.5) + a_4(T_s - 66) + a_5(T_w - 50)] \qquad (9)$$

Since $LT = LpP + LO$, then $a_0 = LO$ and $a_1 = Lp$. The other coefficients are derivatives of LO with respect to each test condition. The term inside the bracket is referred to as the environmental parameter. Other parameters such as model weight and center of gravity can be included as environmental parameters if required. The environmental parameter is only a correction to the coulomb rolling moment and not to the viscous damping moment. By varying the test parameters in the math model individually, an understanding can be gained of how critical it is to control each test condition. For instance, Fig. 10 presents the effects of chamber pressure perturbations from 0.5 psia (i.e., windage or drag) on total damping.

15

Figure 11 presents all the environmental perturbations in terms of energy loss. Knowing energy dissipation to within ± 1 mW was significant for the present investigation; therefore, maintaining a constant vacuum pressure over a long test run can be critical. Applying the correction to actual tare study data is presented in Fig. 12 for a predominant combined Tw and Ts 10°F change. The application of the LT correction reduced the scatter by almost 50 percent. Another advantage of having a tare math model incorporated into the data reduction program is that it can provide a means of correcting for drifting test conditions during a run.

4.6 DAMPING UNCERTAINTY

Several tare runs were obtained initially during the investigation to provide information about the 1DOF bearing's damping uncertainty. Figure 13 represents an overall data repeatability of viscous and coulomb damping. The viscous damping-moment precision error (S) was estimated to be S = ± 0.001 in.-lbf at the maximum roll rate of 700 deg/sec. The coulomb rolling-moment error was estimated to be S = ± 0.0005 in.-lbf over the entire roll rate range. The samples of data presented in Fig. 13 consist of runs obtained days and weeks apart and after extreme variations in test and bearing conditions. Back-to-back runs were obviously much better than the overall uncertainty, but scatter in Fig. 13 is more representative for a typical test matrix execution. Although the data presented in Fig. 13 are precision errors, the "true" bias error is unknown. To estimate the data bias error, the tare model was rotated clockwise (CW) and counterclockwise (CCW) as presented in Fig. 14. At a roll rate of 700 deg/sec the viscous damping moments deviated by B = ± 0.003 in.-lbf. Typically, all data are obtained in one spin direction when determining incremental effects, which eliminates the bias error. The coulomb rolling-moment bias error was estimated to be B = ± 0.0045 in.-lbf. Notice the sign change of LO from spinning CW to CCW. If the coulomb moment were truly independent of spin direction, the magnitude of LO would be identical or, in other words, symmetrical about LO = 0. Differences in the bias estimation might be contributed to spinning against the 1DOF bearing's natural internal flow pattern (i.e., motor forces), and surface imperfections of the 1DOF internal race, the outer tare model surface, turbine vanes, and the holes of the brass counterweight rings, which all can cause turbulent flow disturbances. Additional information about the coulomb rolling-moment bias could also be explained from the results described in Section 4.7.

4.7 COULOMB ROLLING MOMENT

An interesting and unanticipated characteristic of the 1DOF bearing was determined during the investigation. Apparently, the entire bearing system (i.e., tare model/bearing/sting assembly) was sensitive to various types of disturbances. When the bearing system was disturbed, such as removing and installing an EUD, a shift in coulomb rolling moment usually

16

occurred that was several times larger than estimated uncertainty and was nonrepeatable. In one particular instance, the supply pressure was shut off during non-testing hours, allowing the weight of the model to rest on the inner bearing surfaces. When the air was turned on again, a 0.017 in.-lbf LO shift resulted not only in magnitude, but even in direction (Fig. 15) for both runs obtained in CCW directions. Isolation of the component that caused the LO shift was never pursued, but suspect areas are the thrust bearing, locating pins, and/or sting assembly which were altered once the total weight came to rest on the inner bearing surfaces. Minor disturbances such as vacuum pump operation or entrance into the chamber usually caused shifts less than the measurement uncertainties. During the tare study (approximately 15 runs), bearing contact/disturbances were not permitted—only changes in the test conditions. This tends to suggest why the LO value remained approximately − 0.02 in.-lbf during the tare study, as presented earlier in Fig. 13. Thus, the coulomb rolling moment of an EUD could not be established by subtracting the tare math model value from the total EUD damping because of the bearing LO shift.

Fortunately, another method of determining LO of the EUD was devised. The nonrigid EUD was artificially converted to a rigid tare configuration with a special locking device while protecting the bearing system from major disturbances. Afterwards, the EUD was unlocked and restored to a nonrigid configuration, thus allowing a direct data comparison without making a major model change. As presented in Fig. 16, the technique proved beneficial in determining that the EUD coulomb rolling moment was 0.003 in.-lbf, which was outside the 1DOF bearing coulomb rolling-moment precision of ± 0.0005 in.-lbf. For this particular data set, the slight bow in the curve is a typical characteristic for models spinning at atmospheric pressure where LO is proportional to the dynamic pressure.

4.8 VISCOUS DAMPING MOMENT

The 1DOF bearing viscous damping-moment measurement remained to within ± 0.0002 in.-lbf even when subjected to the air-off and air-on disturbance (Fig. 17) that caused the 0.017 in.-lbf LO shift presented in Fig. 15. Since the coulomb rolling moment of the EUD was determined to be minimal (0.003 in.-lbf), the major source of energy dissipation was caused by viscous damping. The EUD viscous damping moment was determined to be significant for a range of test conditions. The ability of the 1DOF technique to distinguish the subtle changes in EUD test conditions relative to a tare run is presented in Fig. 18.

During the investigation there were two rigid tare configurations tested with weights of 183 and 300 lbf, respectively. Both configurations were balanced at the journal bearing center with the same bearing supply conditions. From the laser gap measurements (Fig. 7), it was known that the bearing gap would change, but the effects on damping were unknown. The 1DOF bearing reference tare viscous damping was reduced with increased tare model weight,

as presented in Fig. 19. The additional weight at constant supply pressure most likely altered the journal bearing internal geometry (i.e., boundary conditions) as presented earlier in Fig. 7 for the secondary 1DOF bearing. Correlation of coulomb rolling moment with weight was prohibited because the inherent 1DOF bearing LO shift when the bearing was subjected to major disturbances.

5.0 CONCLUSIONS

An experimental investigation was conducted in the ACL to separate the total rolling moment of rigid and nonrigid mechanical systems into viscous damping and coulomb rolling-moment components. The test technique consisted of measuring roll rate decay of rigid and nonrigid mechanical systems on a 1DOF cylindrical gas bearing. A significant amount of information was collected about the operational characteristics of the 1DOF gas bearing at certain test conditions. The application of the test technique could be beneficial for determining damping properties of other mechanical systems such as turbomachinery, space structures, gas/ball bearings, and high-damping-capacity materials.

Although the real significance of this investigation might be perceived to be in the technical results, the investigation also deserves attention in the areas of test technique, measurement accuracy, enhancement of test hardware, and meeting the investigation objectives in a laboratory environment with minimal associated risks and costs. Aspects of the test not discussed here which provided the necessary foundation for a successful investigation are the technical knowledge, initiative, creativity, test experience of the personnel, and the unique ACL facility and other hardware that exist at AEDC.

The following conclusions are based on the investigation results:

1. The ACL was again demonstrated to be a viable laboratory for research and development at AEDC because of its inexpensive operation, flexibility to adapt to different test-peculiar requirements, and conducive atmosphere for technical advances.

2. A test technique was developed and demonstrated to be successful for measuring viscous damping and coulomb rolling moment of a 1DOF gas bearing and nonrigid mechanical systems. During the investigation, significant characteristics and operational capabilities of the 1DOF bearing were noted as follows:

   ● Viscous damping-moment uncertainty of ± 0.001 in.-lbf or ± 1 mW energy dissipation was achieved.

● Previous roll rate uncertainties of ± 1 deg/sec were improved by two orders of magnitude to ± 0.01 deg/sec by circumventing the frequency-to-voltage converter and acquiring data with accurate timers in a digital format. The use of accurate timers also improved roll moment of inertia measurements to ± 0.01 percent.

● A math model was developed by using a multiple linear regression scheme to correct for environmental changes of the 1DOF bearing tare damping moment.

● The journal bearing spring stiffness was determined by using a laser-optic sensor to measure the film gap displacement profiles. The displacement profiles were used to estimate angular and radial natural frequencies and operable spin rates.

● Coulomb rolling-moment shifts were experienced with the 1DOF bearing during major model changes and were nonrepeatable.

● In contrast to the secondary 1DOF bearing fabricated completely from 440B stainless steel, the 1DOF bearing fabricated from Armco, Kennertium-W2, and 440B stainless steel had relatively large film gap variations when it was subjected to steady-state temperature changes or gradients.

6.0 RECOMMENDATIONS

The following recommendations are based on the present performance and related experience with the 1DOF gas bearing. These recommendations should be seriously considered for future tests at AEDC that intend to use a 1DOF gas bearing for mechanical system damping measurements.

1. Further investigations are required to identify the source of the coulomb moment shift that was experienced during the investigation. Unless a mechanical system being tested has a built-in feature to avoid major disturbances to the 1DOF bearing, a coulomb rolling-moment shift may result and prohibit test objectives from being obtained.

2. State-of-the-technology 1DOF gas bearings exist with negligible and stable coulomb rolling moment. A bearing of this type should be procured to supplement and/or replace existing bearings. The new bearing should have a higher radial, angular, and axial stiffness with increased normal and axial load capacity. A target mass flow rate of 0.01 lbm/sec or less is recommended to allow lower ACL chamber pressures to be obtained, thus improving tare damping measurements. The bearing should also be able to operate over a large range of steady-state supply temperatures (i.e., 60 to 180°F) and maintain a constant film gap.

3. To improve on roll rate uncertainties, a precision-machined single-spot or multiple-spot tachometer ring would be required. With a precision tachometer ring and new bearing, it should be possible to resolve energy dissipation of mechanical systems within less than ± 1 mW.

REFERENCES

1. Hodapp, A. E. "Evaluation of a Gas Bearing Pivot for a High Amplitude Dynamic Stability Balance." AEDC-TDR-62-221 (AD-290 948), December 1962.

2. Hodapp, A. E., Jr. "A Theoretical and Experimental Investigation of a Spherical Gas Journal Bearing." Master's Thesis, The University of Tennessee, Knoxville, 1967.

3. Burt, G. E. "Design of a Wind-Tunnel Roll-Damping Balance Incorporating Externally Pressurized Gas Bearings Operating at Large Film Reynolds Numbers." AEDC-TR-69-204, (AD-694 502), October 1969.

4. Schueler, C. J., Ward, L. K., and Hodapp, A. E. "Techniques for Measurement of Dynamic Stability Derivatives in Ground Test Facilities." AGARDograph 121, October 1967.

5. Marquart, E. J. "Free Spin Damping Measurement Technique." AIAA 11th Applied Aerodynamics Conference, AIAA-93-3457.
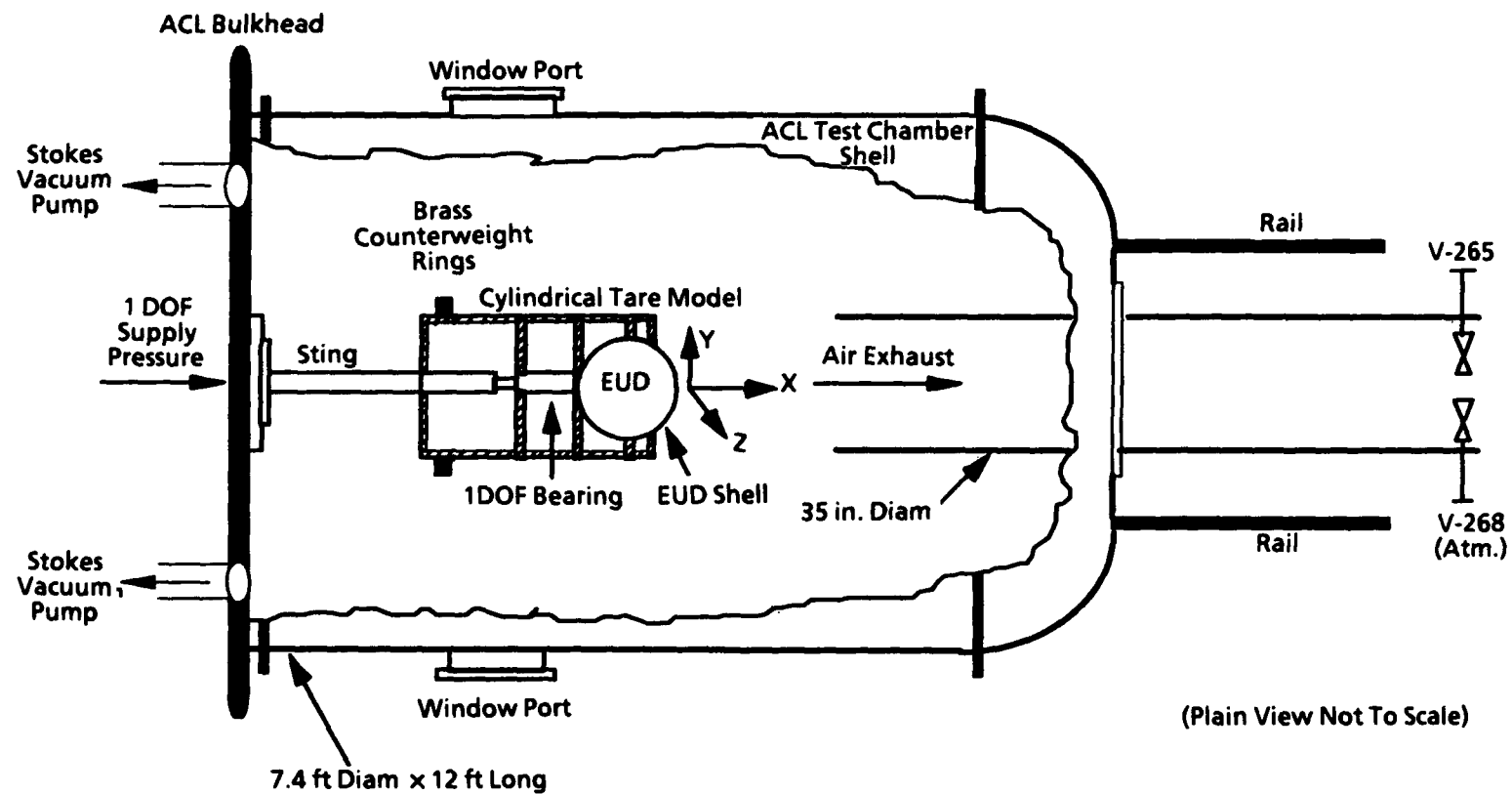
Figure 1. Airflow Calibration Laboratory (ACL).
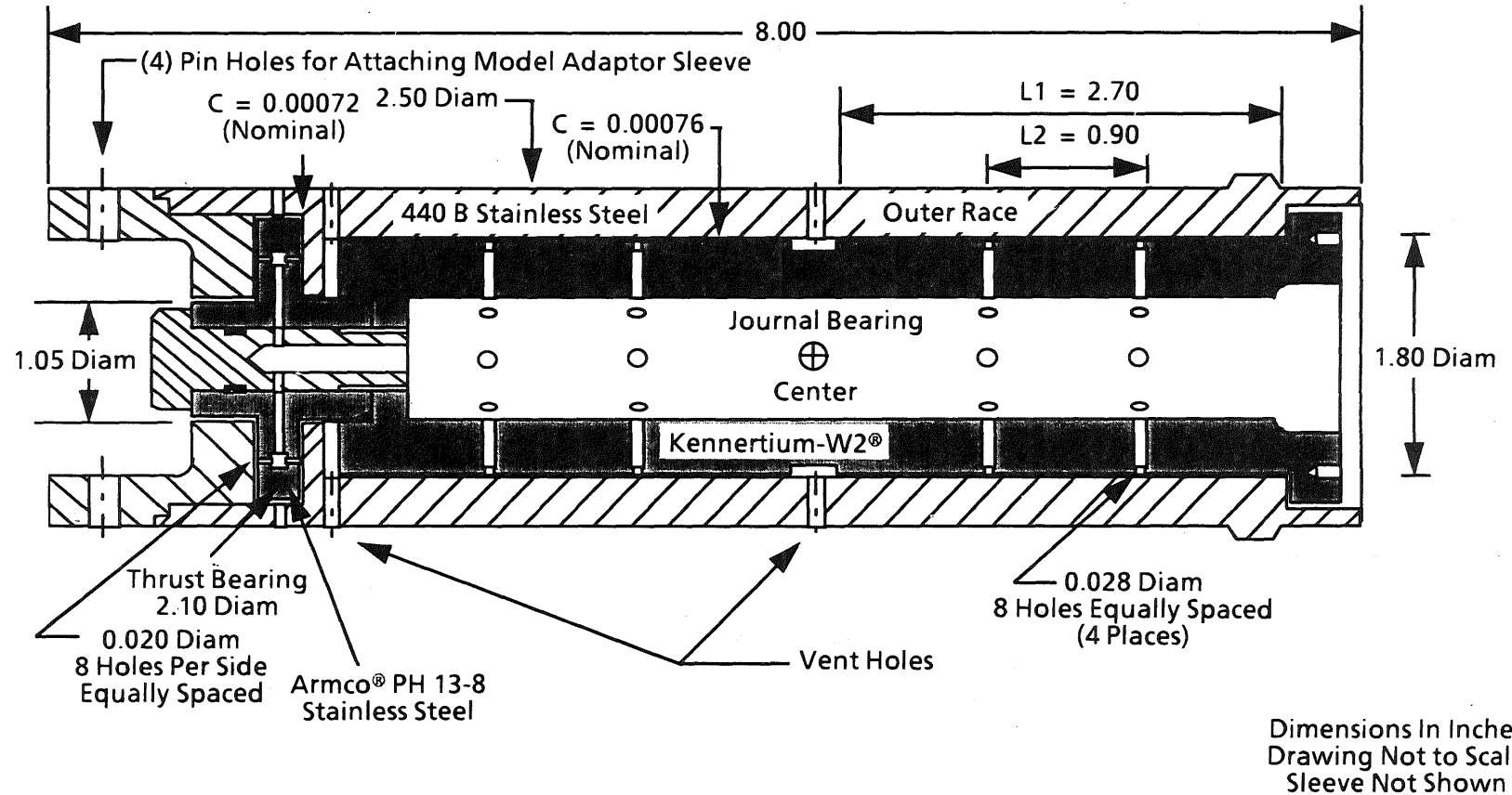
Figure 2. Gas bearing cross-section details.

Cylindrical Tare Body

Brass Counterweight Ring

EUD Shell

Schrader Valve

Vacuum/Backfill Line

AEDC
92-198602
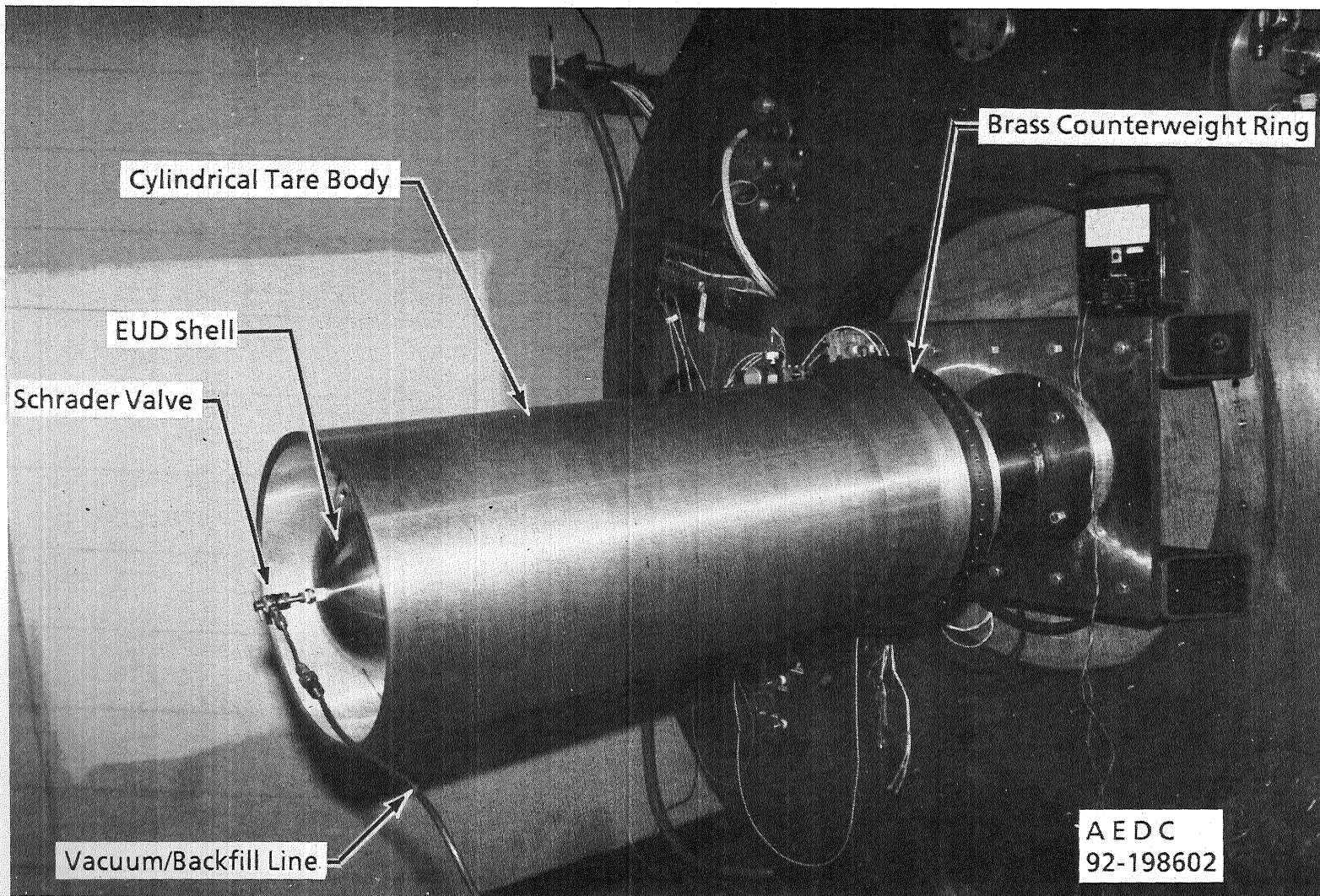
a. Tare body
Figure 3. Model installation in ACL.
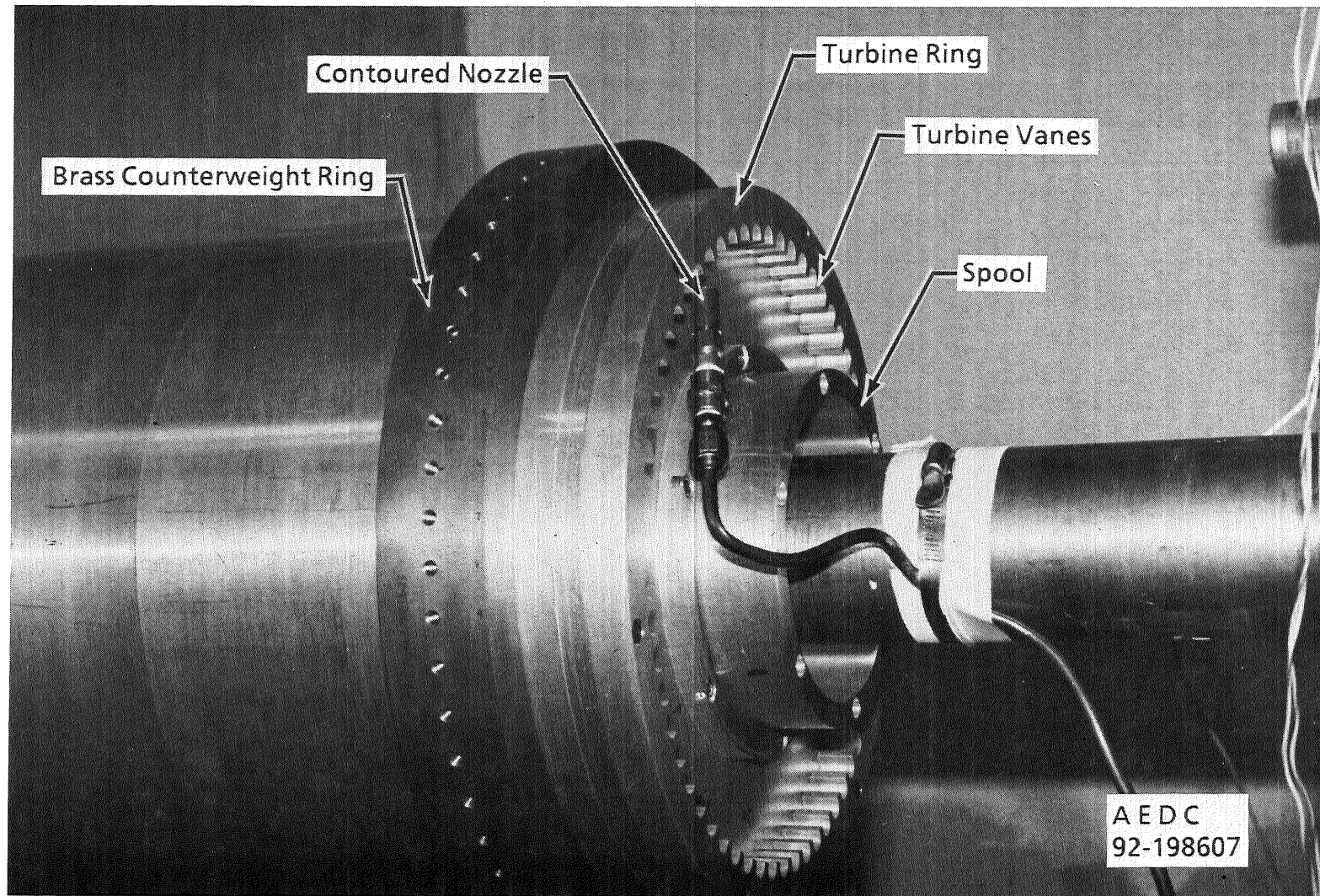
b. Turbine
Figure 3. Concluded.
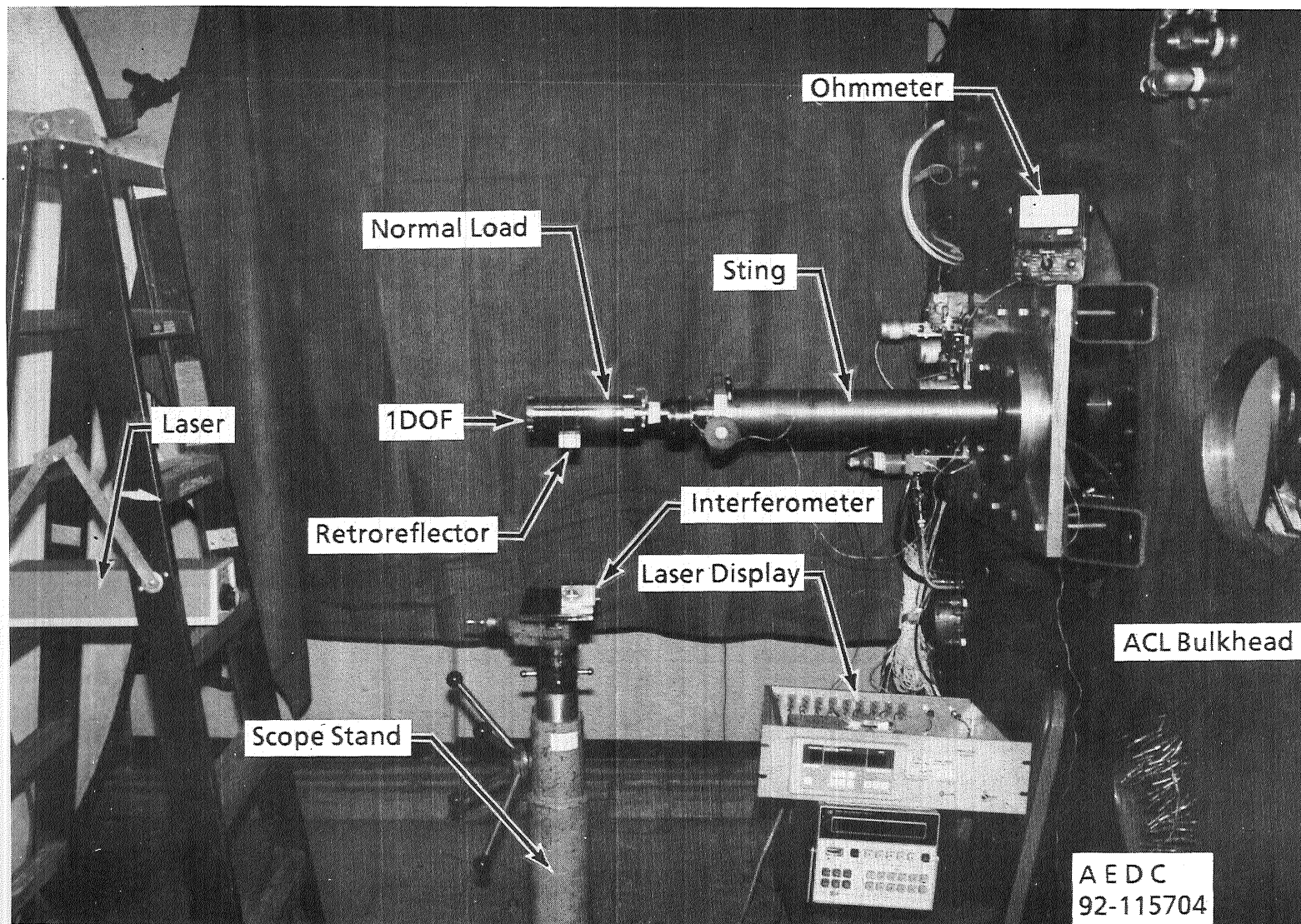
Figure 4. Laser/1DOF installation in ACL.
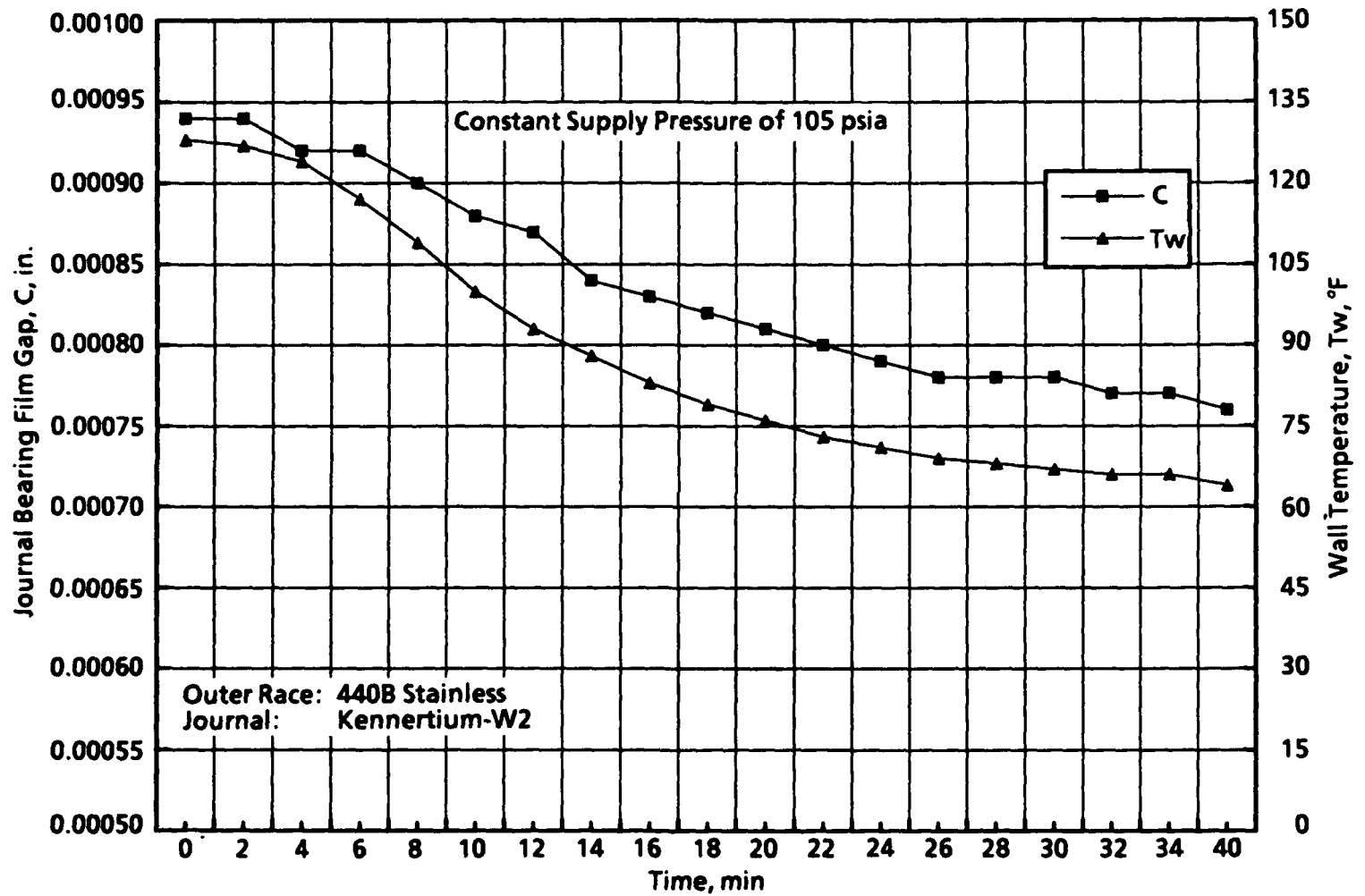
Figure 5. Thermal gradient effects to film gap.
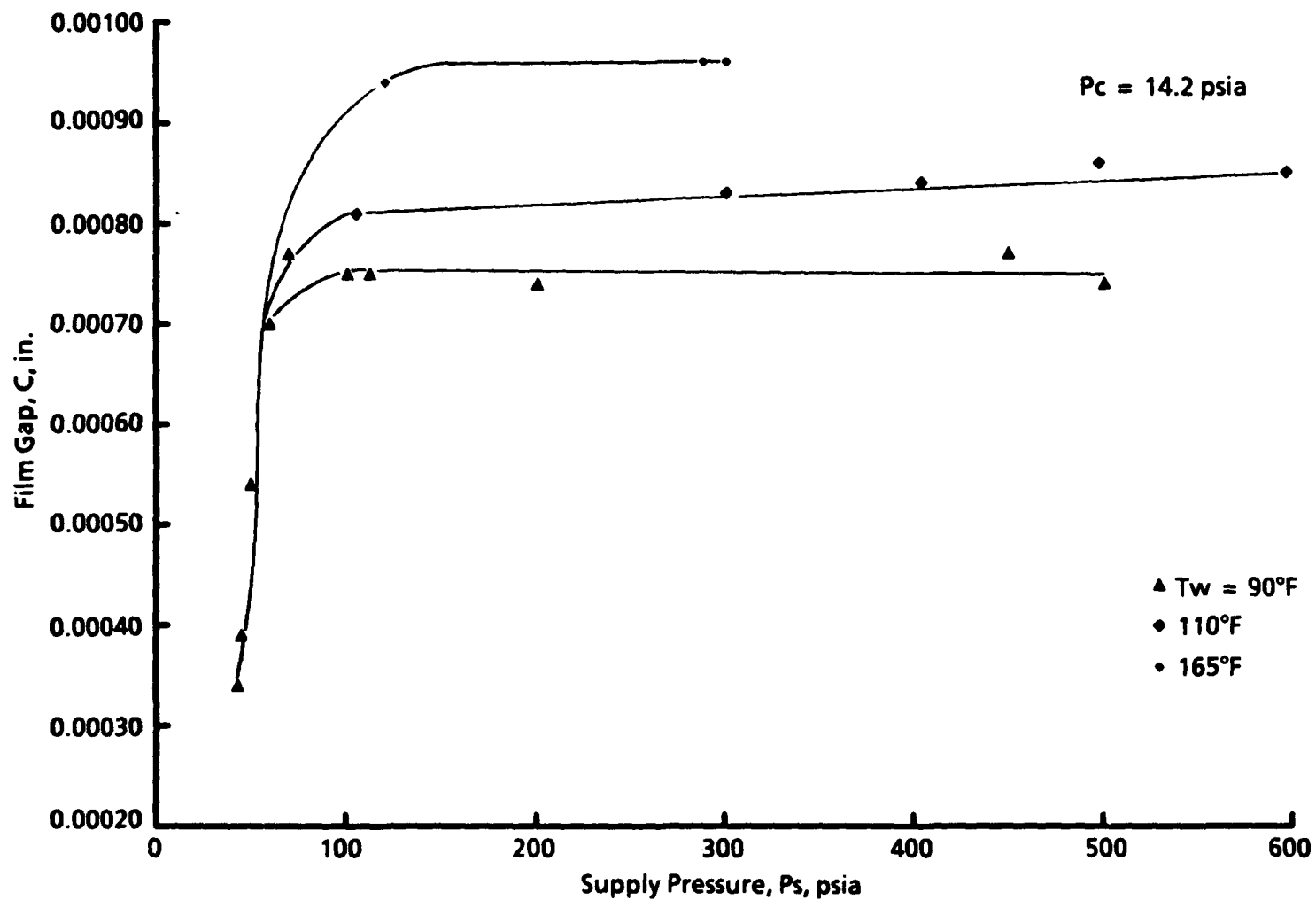
Figure 6. Unloaded film gap profiles at steady-state temperatures.
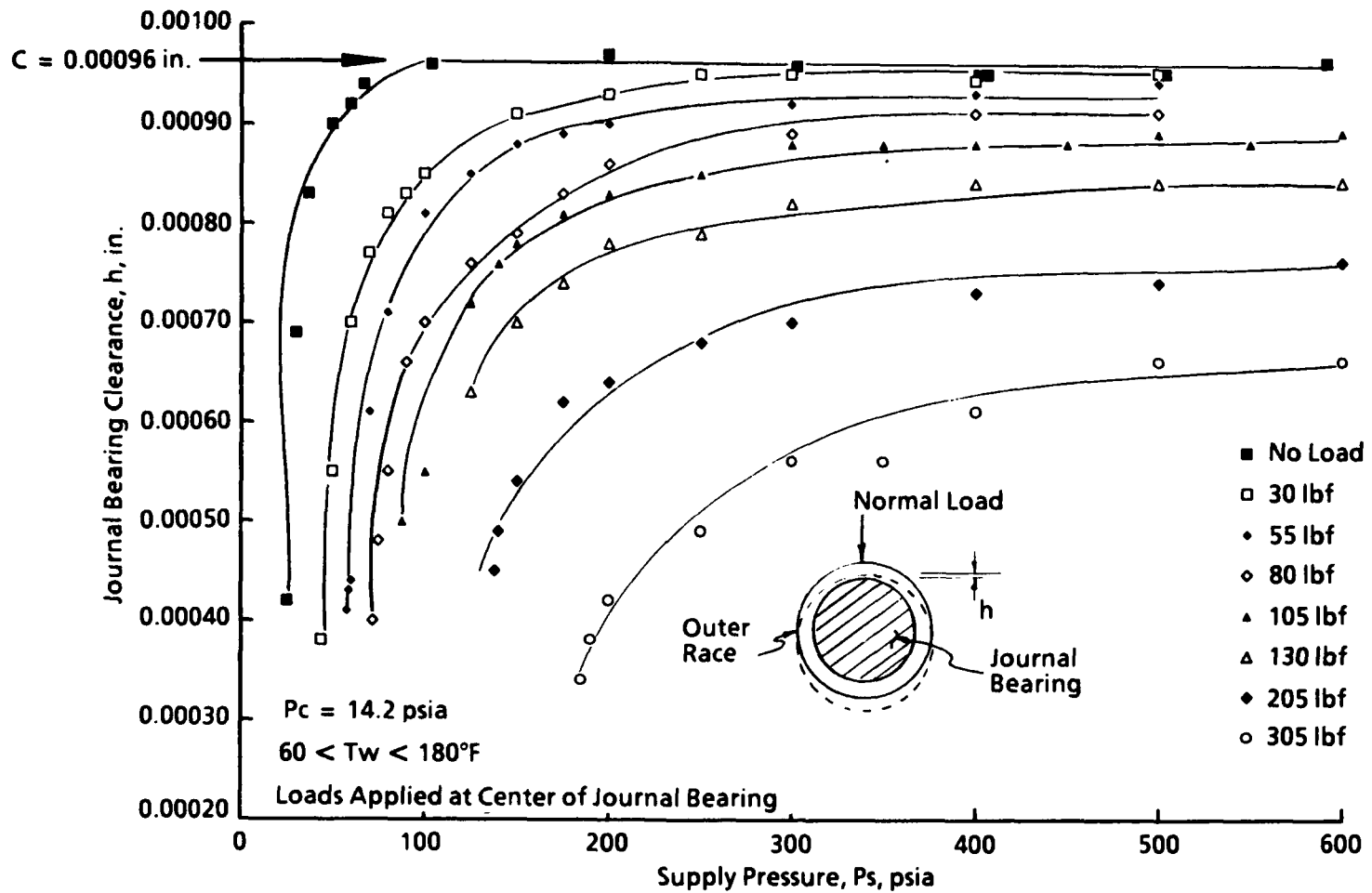
Figure 7. Secondary journal bearing applied load clearance profiles.
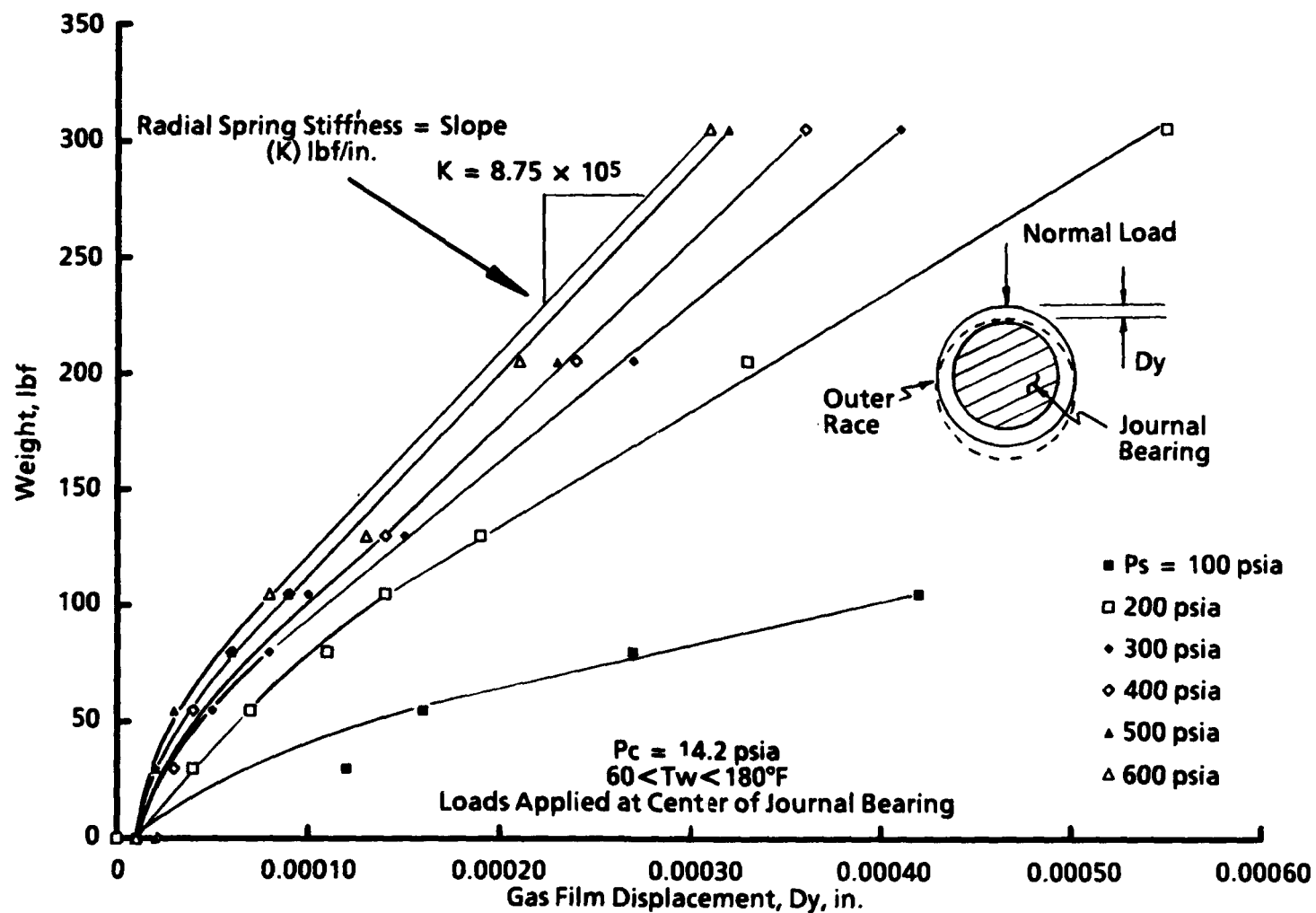
Figure 8. Journal bearing radial spring stiffness.
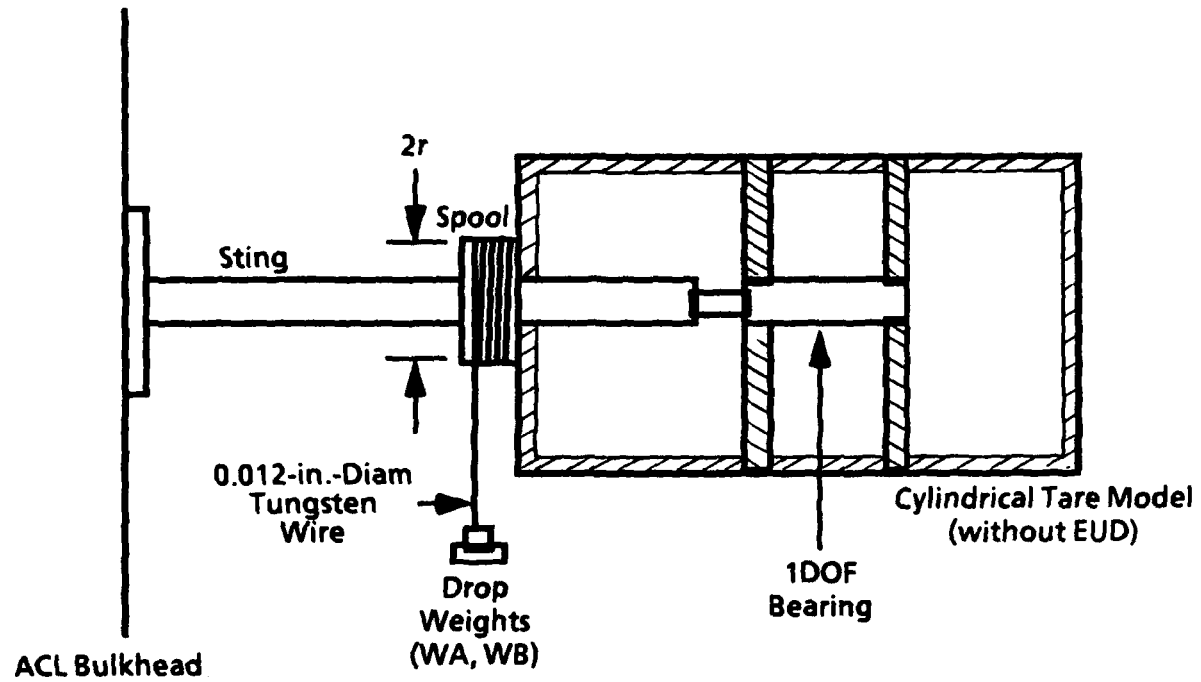
Figure 9. Experimental setup for roll moment of inertia measurements.
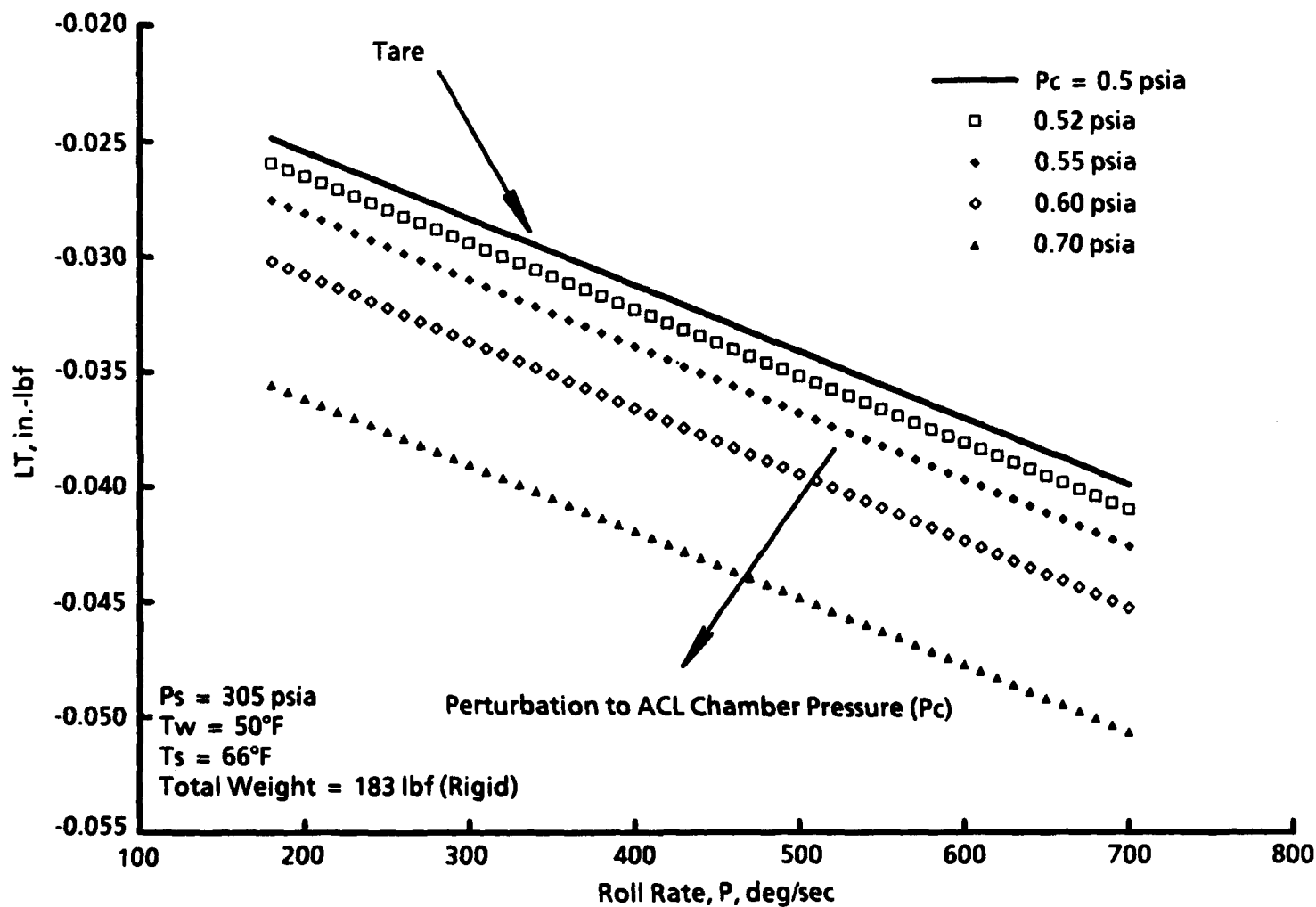
Figure 10. Tare model rolling-moment profiles for chamber pressure perturbations.
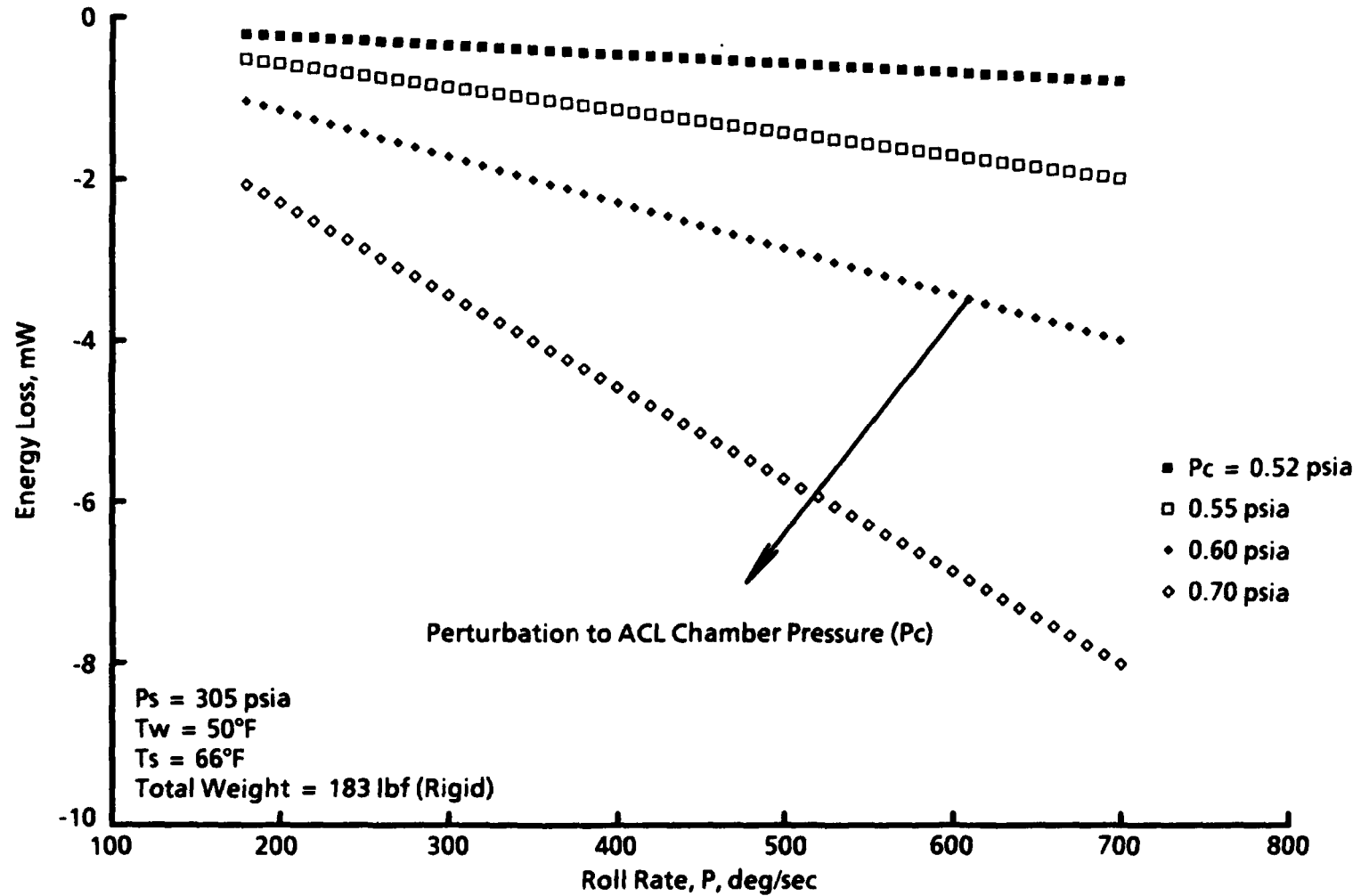
a. Chamber pressure
Figure 11. Energy dissipation for environmental perturbations.
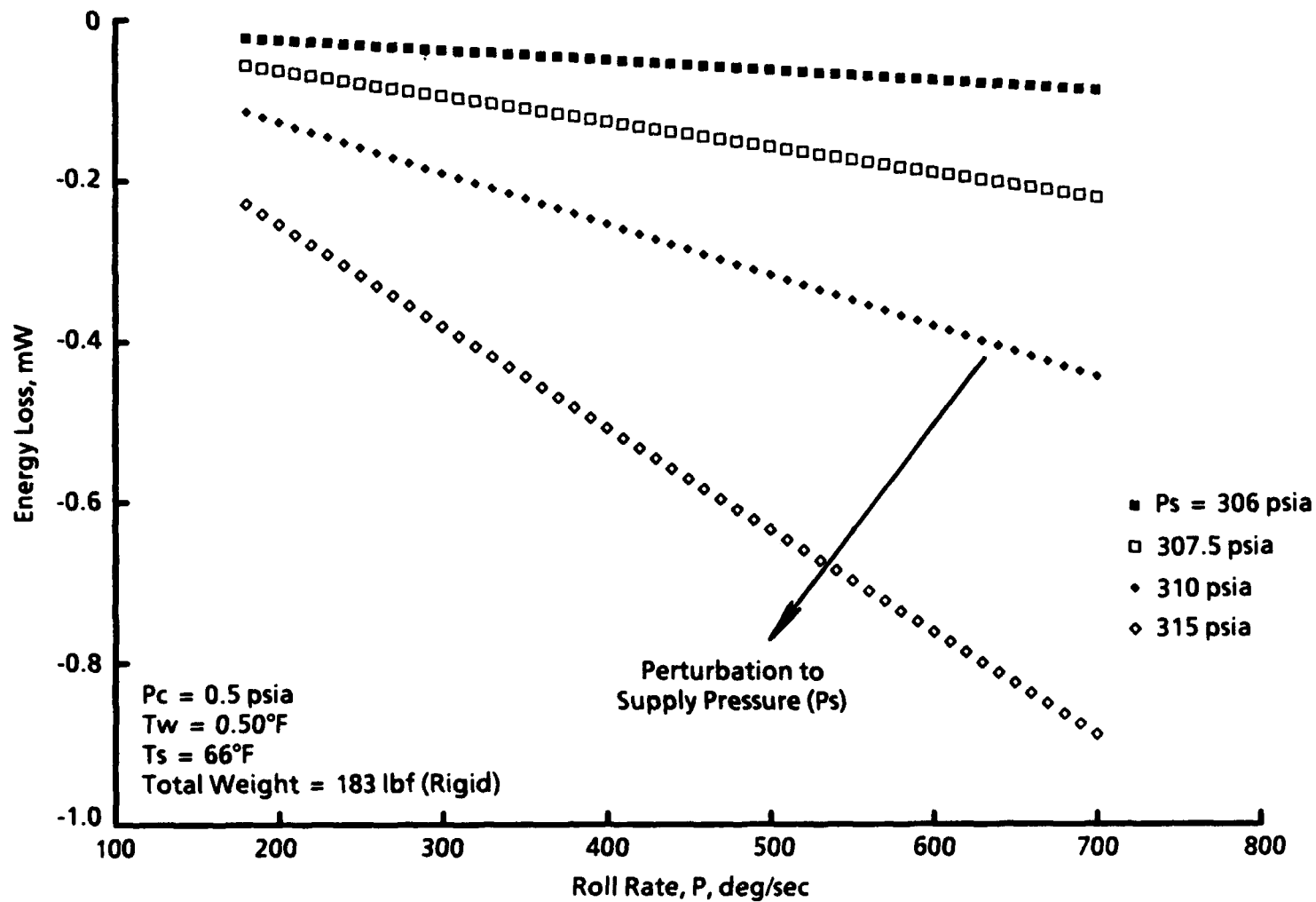
b. Supply pressure
Figure 11. Continued.
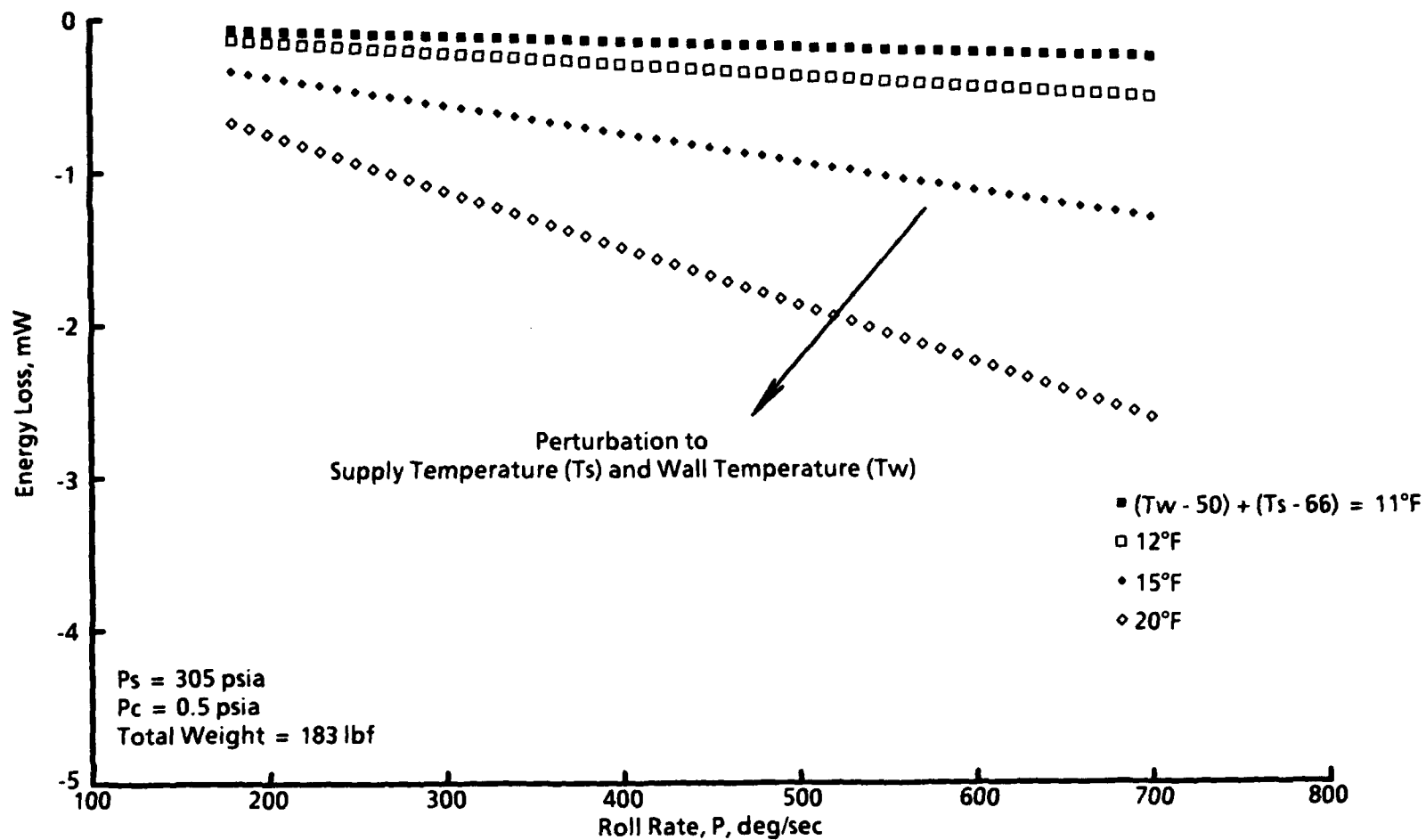
c. Supply and wall temperature
Figure 11. Concluded.
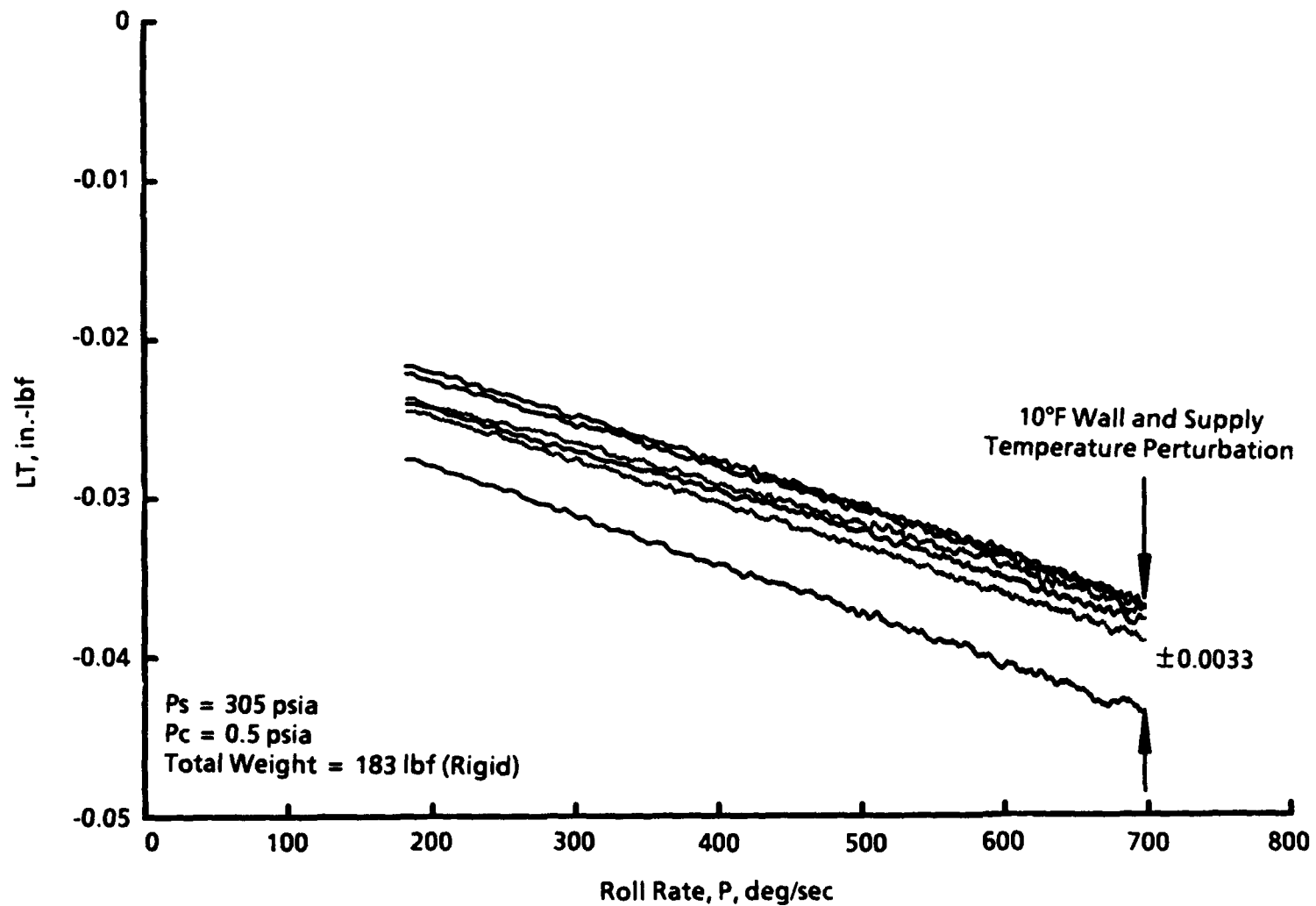
a. Uncorrected

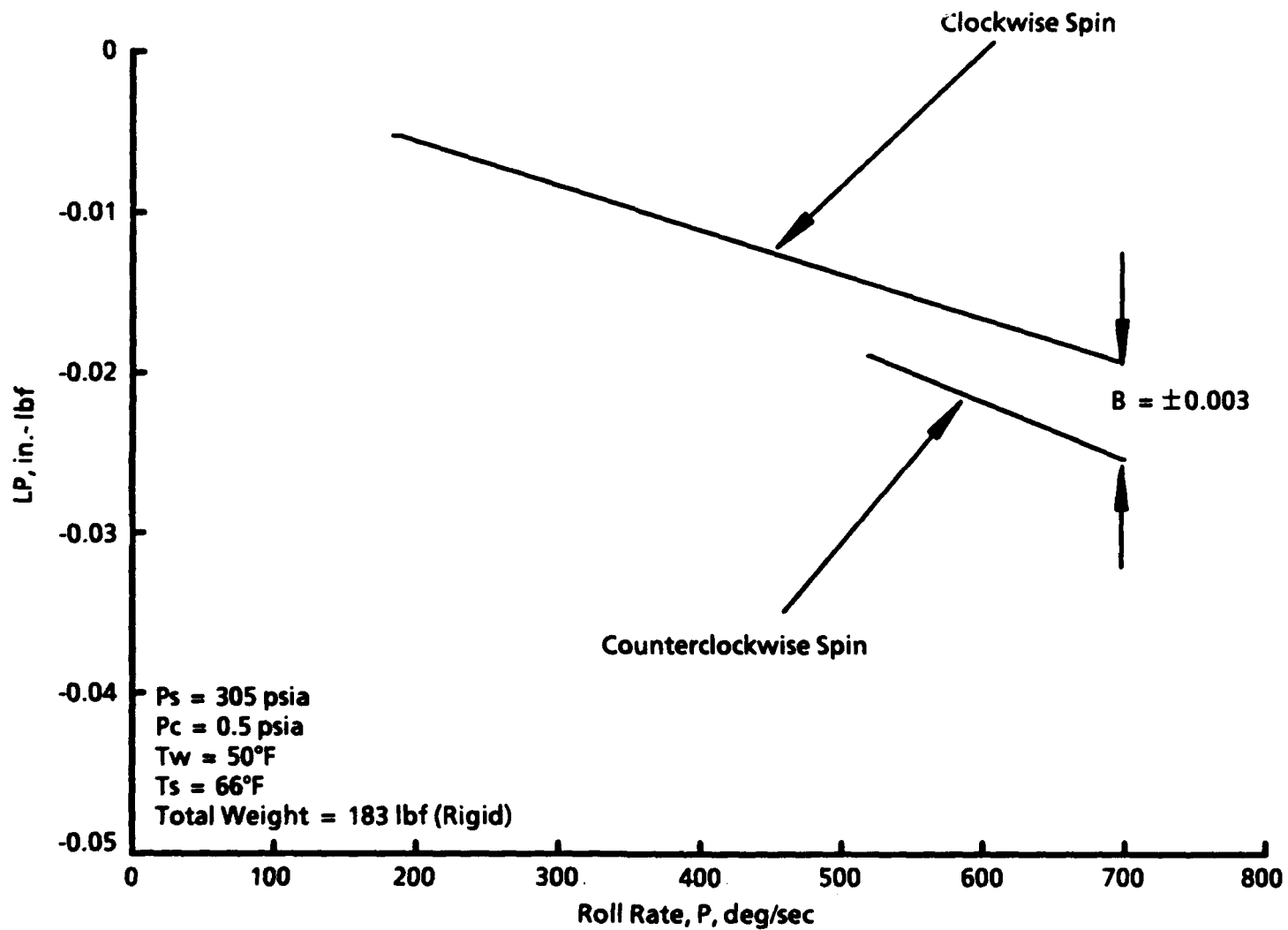Figure 12. Application of the tare math model for temperature perturbations.
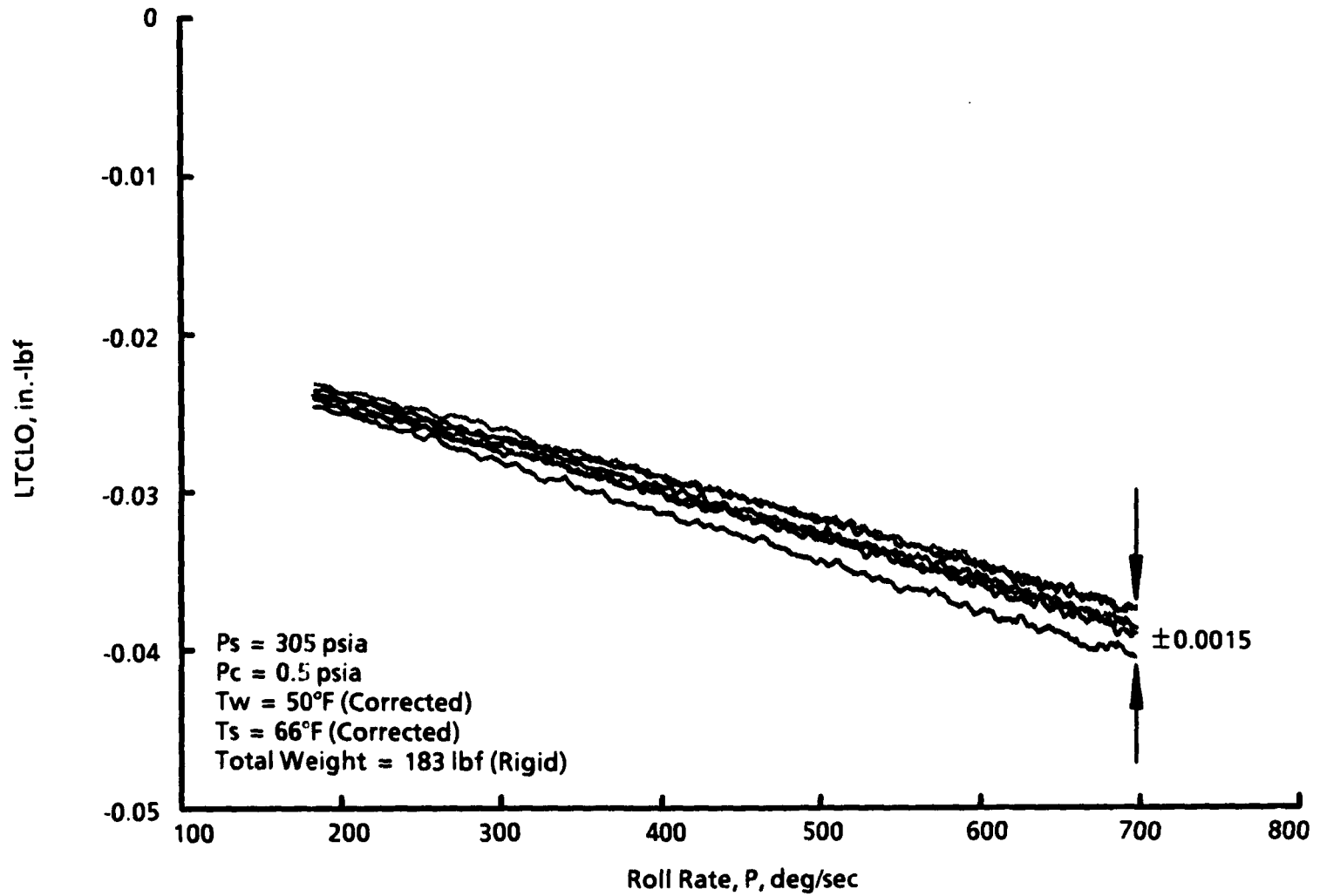
b. Corrected for temperature perturbations
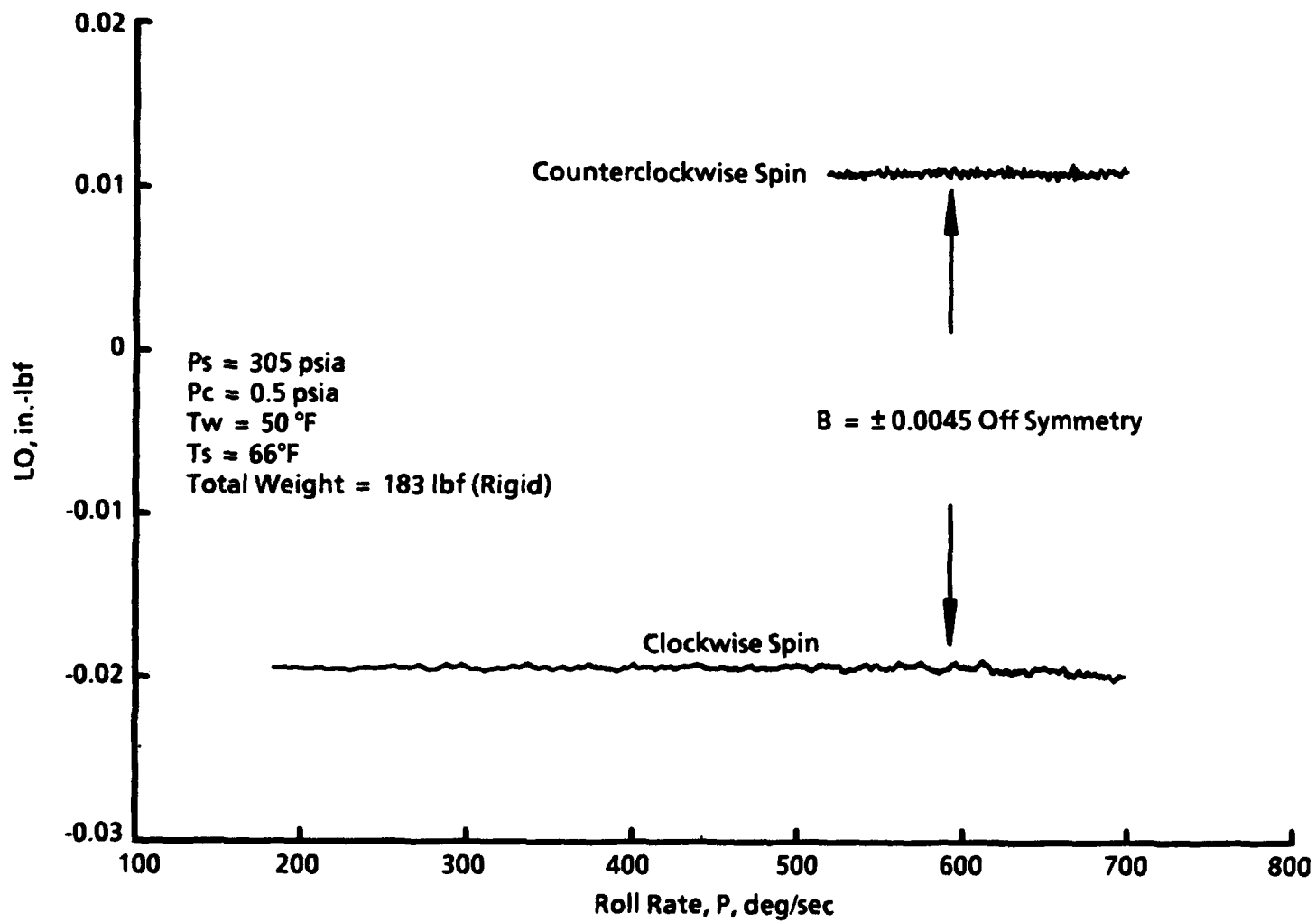Figure 12. Concluded.
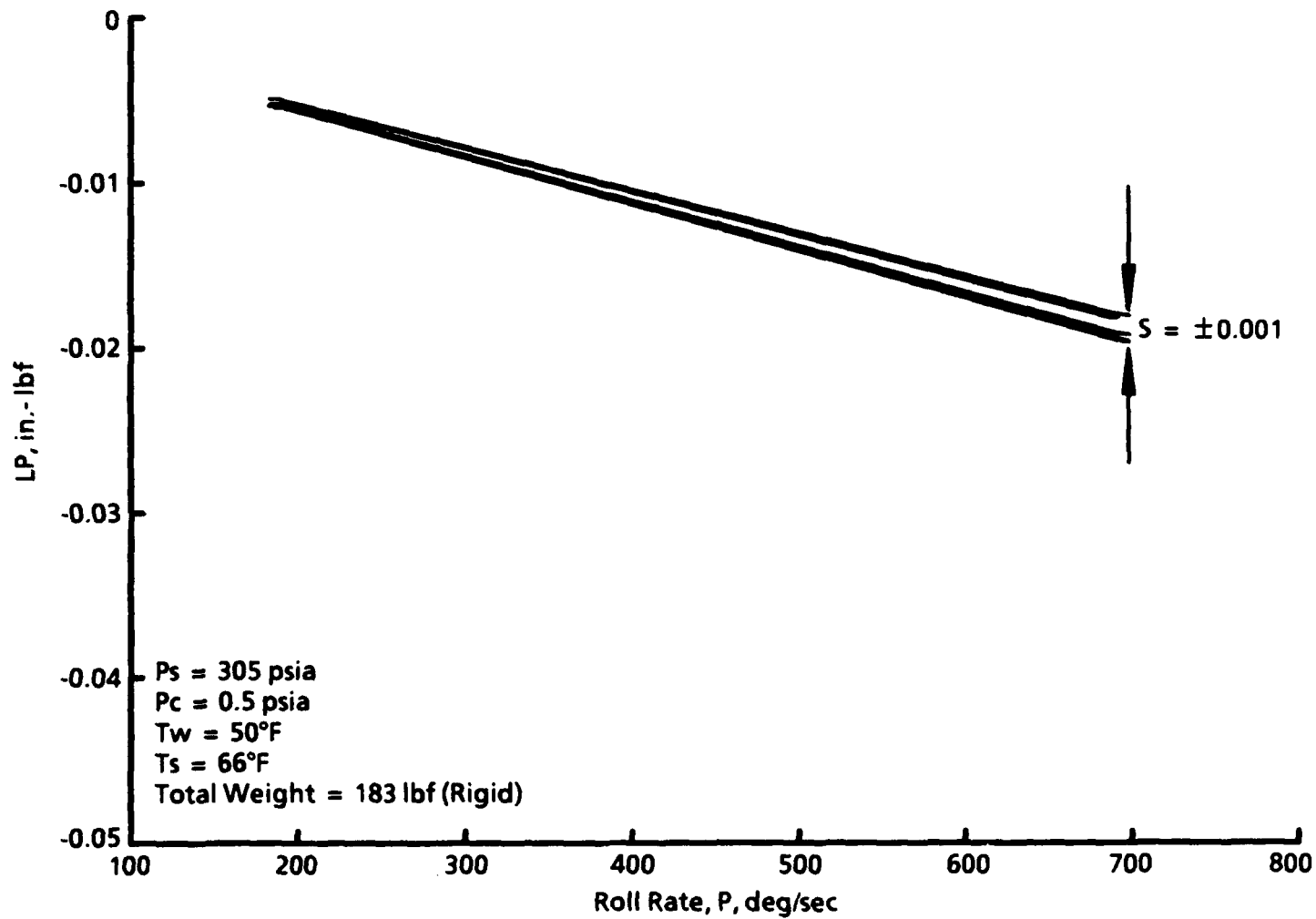
a. Viscous damping moment
Figure 13. Tare precision.
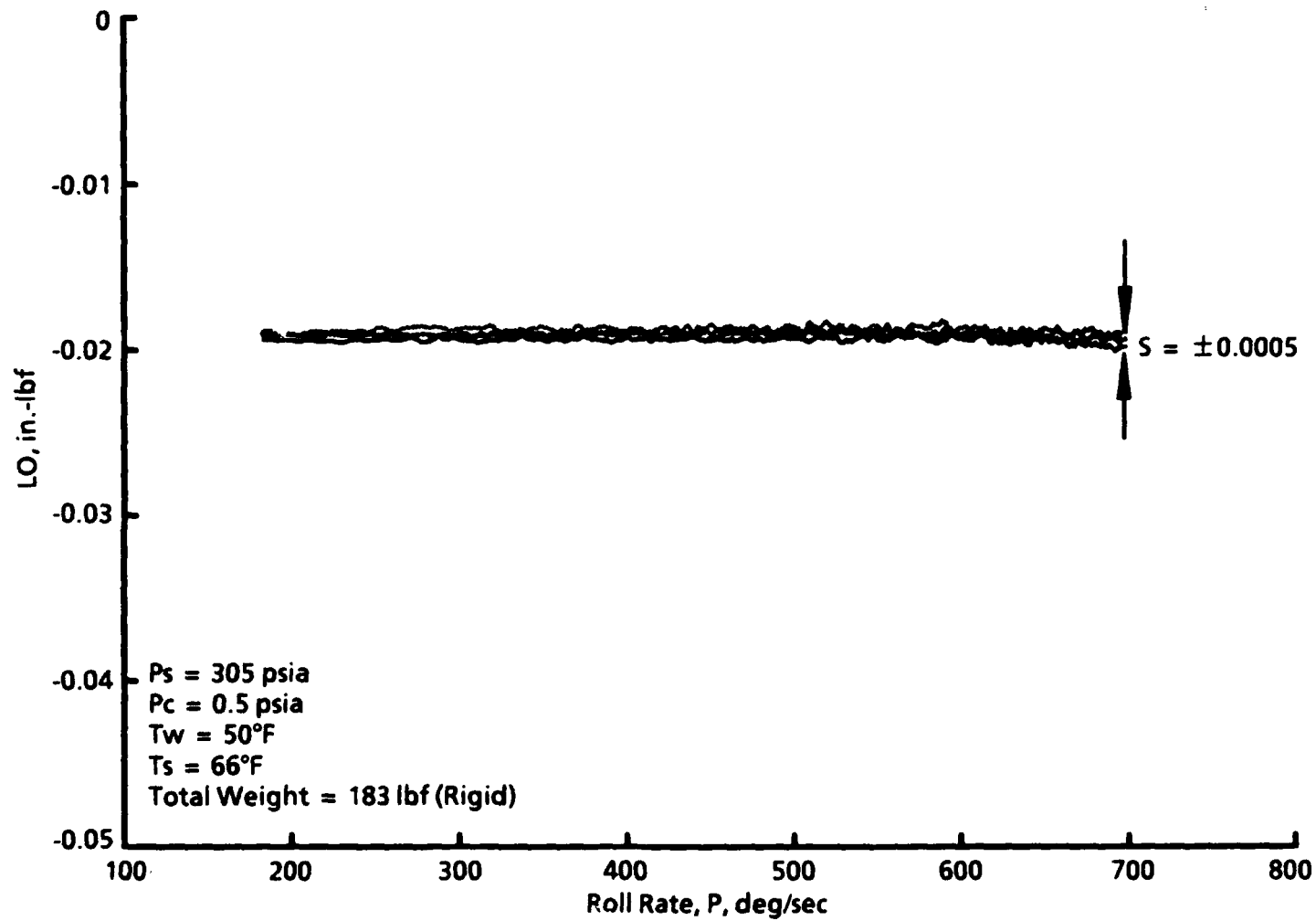
b. Coulomb rolling moment
Figure 13. Concluded.

a. Viscous damping moment
Figure 14. Estimation of tare bias.
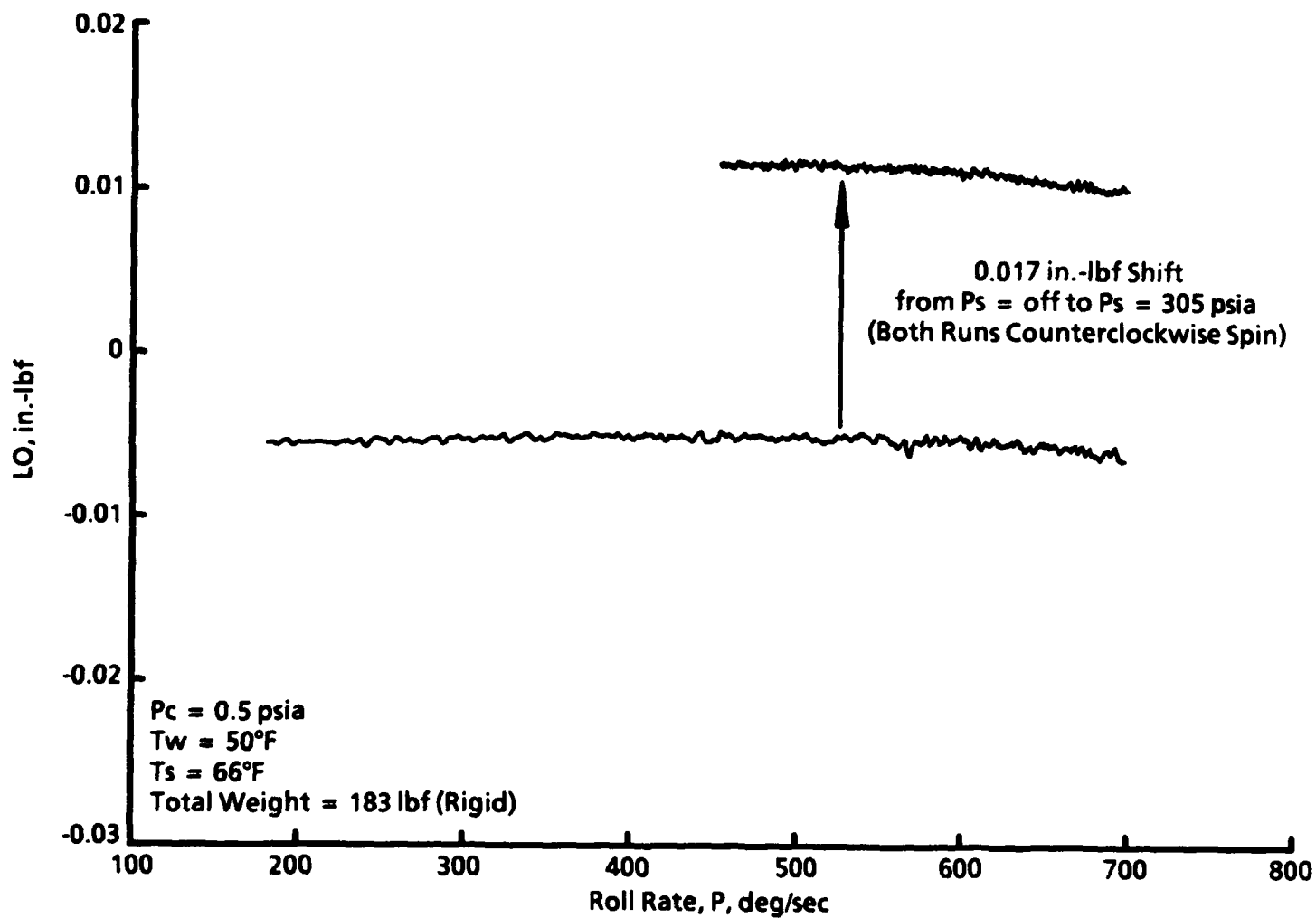
b. Coulomb rolling moment
Figure 14. Concluded.

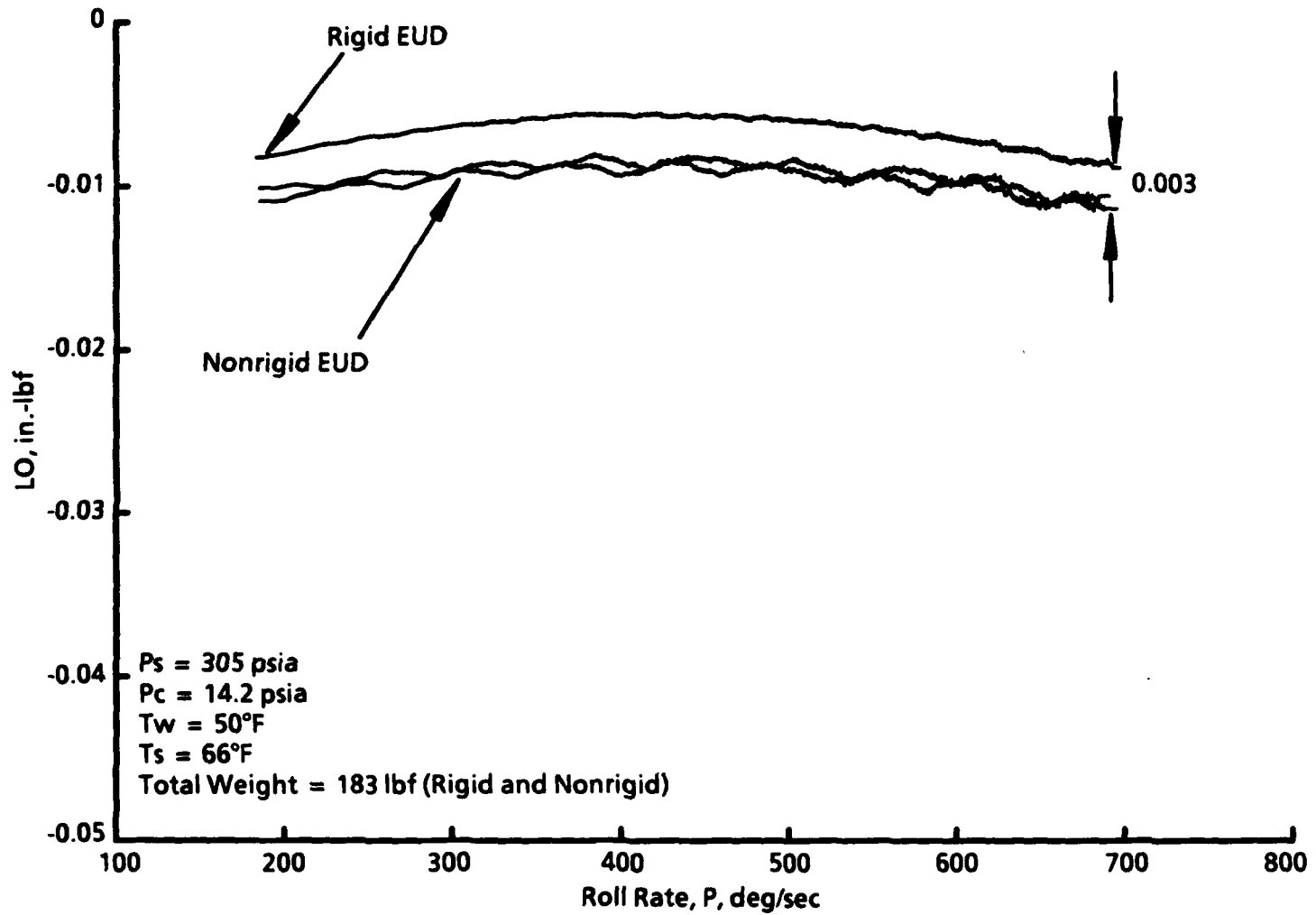Figure 15. Repeatability of coulomb rolling moment with supply pressure disturbance.

Figure 16. Internal coulomb rolling moment of an Engineering Unit Dissipator (EUD).
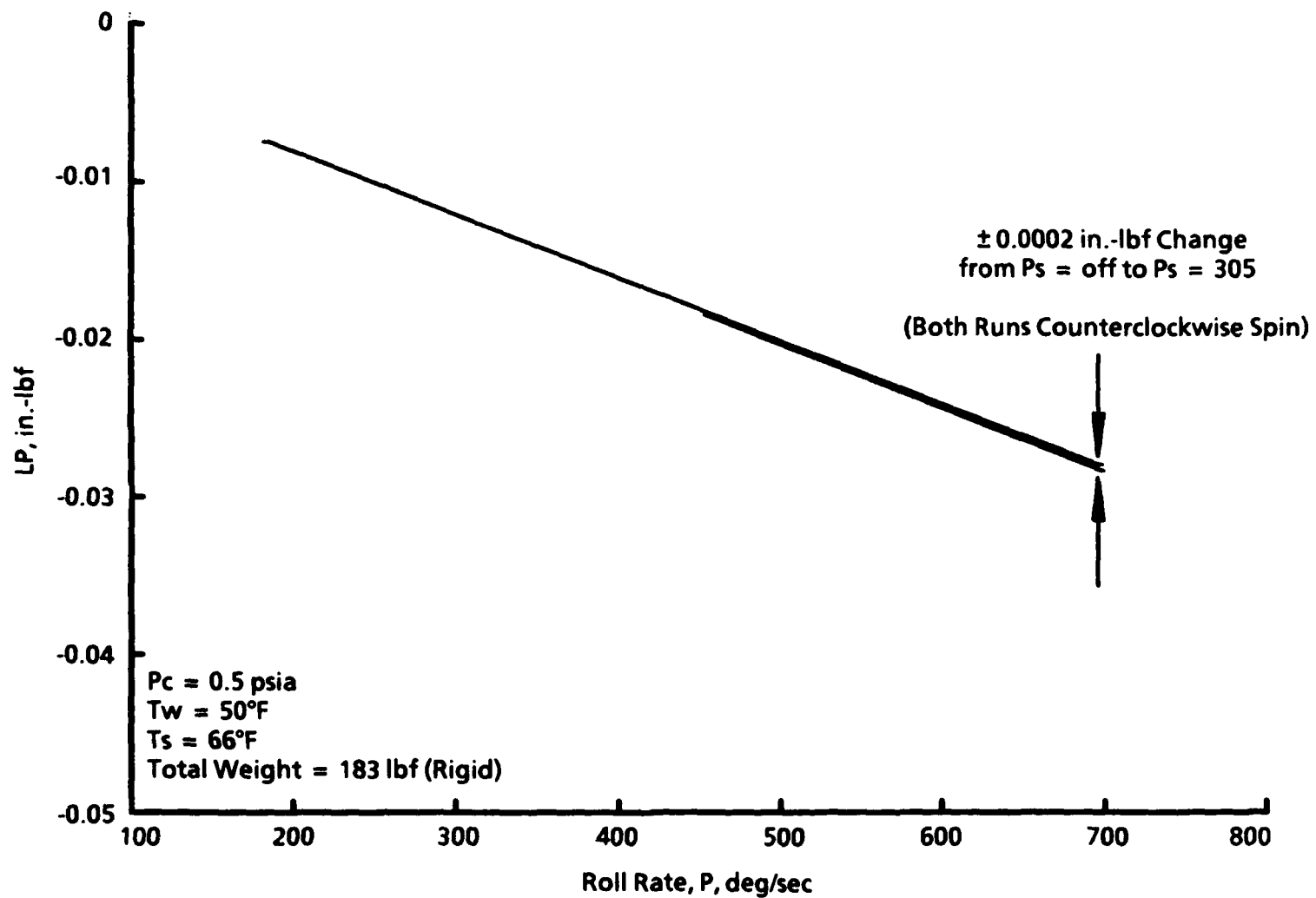
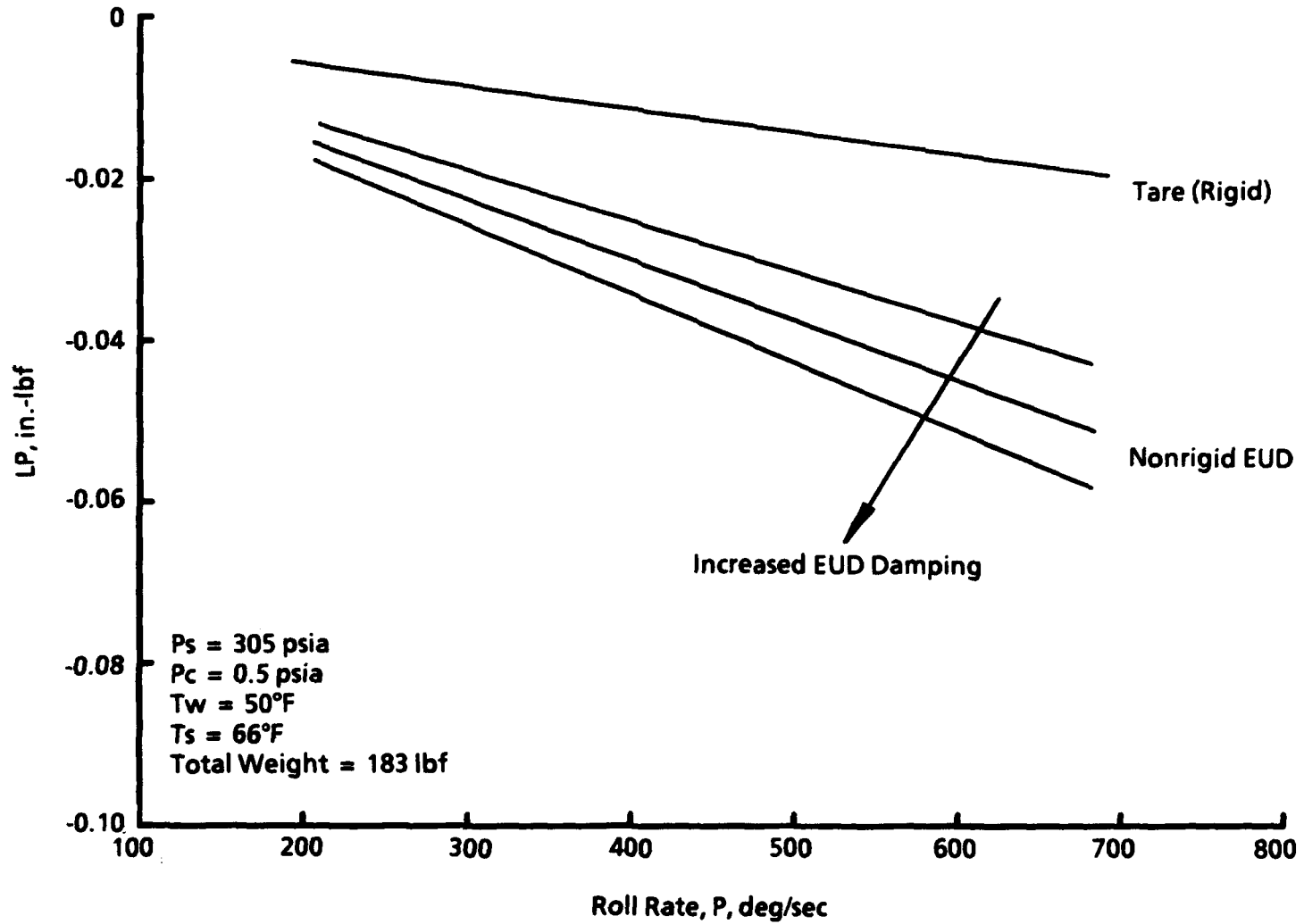Figure 17. Repeatability of viscous damping moment with supply pressure disturbance.

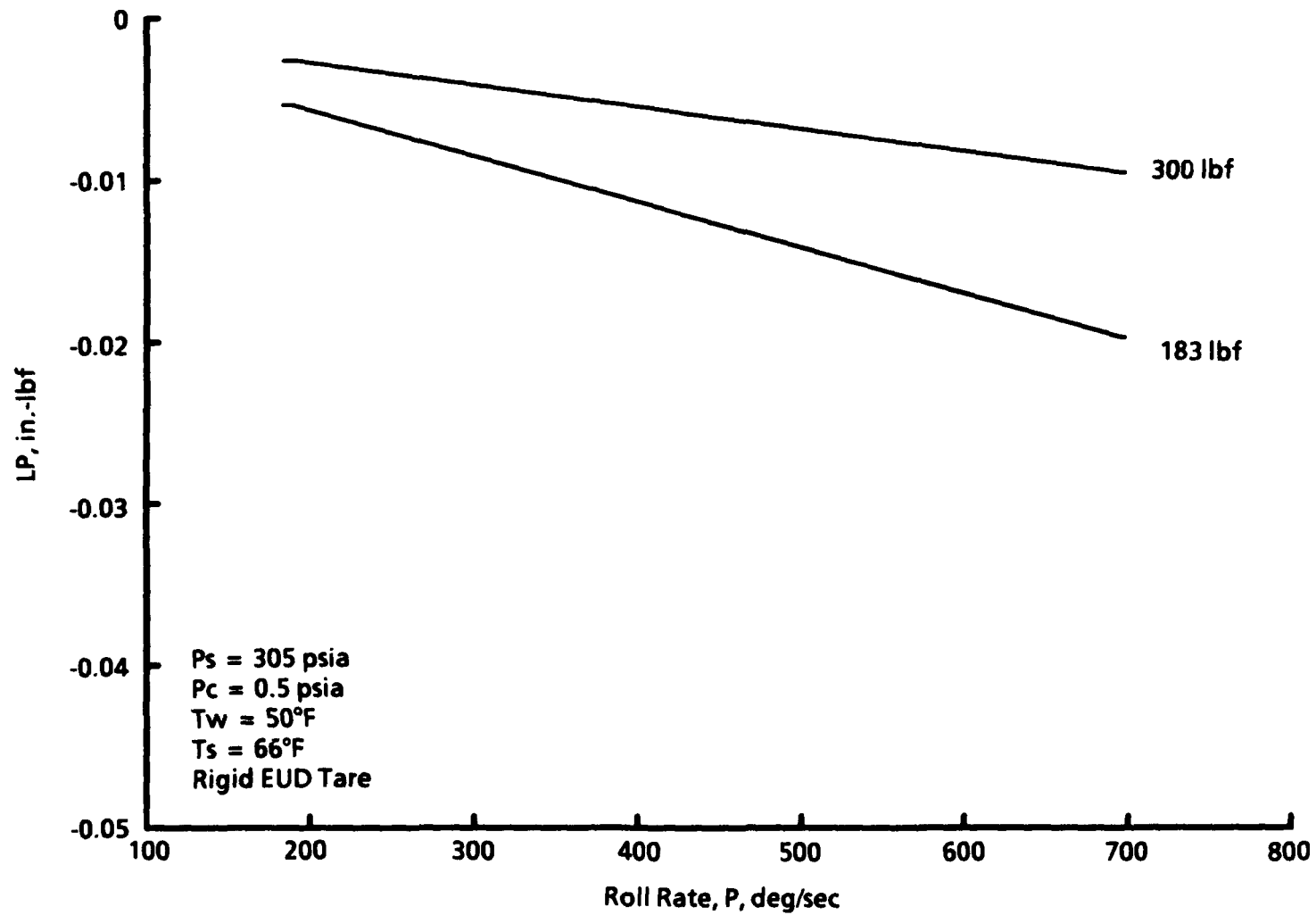Figure 18. Typical viscous damping-moment characteristics of a nonrigid EUD.

Figure 19. Weight effects to the 1DOF bearing viscous damping moment.

Table 1. Estimated Instrumentation Uncertainties

Measurement	Uncertainty	Range	Type of Device
Roll Rate, deg/sec	± 0.01	180 to 720	IR Emitting Photodiode
Supply Pressure, psi	± 0.5	0 to 350	0 - 1,000 Druck®
Supply Temperature, °F	± 2.0	40 to 100	Chromel® -Alumel®
Chamber Pressure, psi	± 0.01	0.5 to 14.2	0 - 15 Druck®
Dewpoint Temperature, °F	± 1.0	−70 to −15	EG&G®
Mass Flow Rate, lbm/sec	± 0.006	0 to 0.125	Kurz®
Time, sec	± 1.0E−06	0 to 2	HP 5316A Counter
Laser/Optics, in.	± 1.0 E−05	0 to 12	HP 5528A

Table 2. Nominal Operating Conditions

Ps, psia	Ts, °F	Tw, °F	Pc, psia	P, deg/sec
305	66	50	0.500	700 - 180

NOMENCLATURE

1DOF	One-degree-of-freedom gas bearing
ACL	Airflow Calibration Laboratory test chamber
a	Tare model roll acceleration, ft/sec^2
$a_0, a_1, \ldots a_5$	Least-squares curve-fit coefficients
a_A, a_B	Average tare model acceleration for A and B, respectively, ft/sec^2
B	Bias error for uncertainty measurements, in.-lbf
C	Bearing clearance (gas film thickness) at no load, in.
Dy	Journal bearing displacement from the no-load position, in.
EUD	Engineering Unit Dissipator model
g	Local acceleration of gravity (32.140978), ft/sec^2
h	Journal bearing applied load radial clearance at the normal load point, in.
I_{xx}	Mass moment of inertia about the x-axis, slug-ft^2
K	Radial spring stiffness of the journal bearing, lbf/in.
L	Damping moment, ft-lbf
L1	Journal bearing pad length, in.
L2	Distance between journal bearing orifice rows, in.
LO	Total nonconstant coulomb rolling moment, ft-lbf
Lo	Constant coulomb rolling moment, ft-lbf
LP	Total viscous damping moment, ft-lbf

Lp	Viscous damping-moment parameter, ft-lbf-sec/rad
LT	Total rolling moment, ft-lbf
LTCLO	Total rolling moment corrected for LO environmental effects, in.-lbf
P	Model roll rate, rad/sec
$\dot{P}$	Model roll acceleration, rad/sec^2
Pc	ACL chamber static pressure, psia
P_i	Initial roll rate for data acquisition, rad/sec
Ps	Bearing supply pressure, psia
P_{ss}	Steady-state roll rate, rad/sec
r	Radius of moment of inertia spool and drop weight wire, in.
S	Precision error for uncertainty measurements, in.-lbf
t	Time of data acquisition, sec
t_i	Initial time of data acquisition, sec
Ts	Bearing supply temperature, °F
Tw	Bearing wall temperature, °F
W_A, W_B	Weight of applied loads for I_{xx} measurements, lbf
X,Y,Z	Cartesian coordinates
ϕ, $\dot{\phi}$, $\ddot{\phi}$	Model roll position, roll rate, and roll acceleration, respectively, rad, rad/sec, rad/sec^2